June 2021

The Feasibility of 18F-FDG Labeled RBC and PET/CT Imaging Blood Perfusion and Vascular Dysfunction Measurements in Pre-clinical Research

Shaowei Wang
University of South Florida

The Feasibility of 18F-FDG Labeled RBC and PET/CT Imaging Blood Perfusion and Vascular Dysfunction Measurements in Pre-clinical Research

by

Shaowei Wang

A dissertation submitted in partial fulfillment
of the requirements for the degree of
Doctor of Philosophy in Biomedical Engineering
Department of Medical Engineering
College of Engineering
University of South Florida

Co-Major Professor: Jung Choi, M.D.
Co-Major Professor: Huabei Jiang, Ph.D.
Mikalai Budzevich, Ph.D.
David Morse, Ph.D.
Mark Jaroszeski, Ph.D.

Date of Approval:
June 10, 2021

Keywords: Myocardial Infarction (MI), Diabetes, Molecular Imaging, Myocardial Vascular, Microvascular Disease

Dedication

This dissertation is dedicated to my family, friends, and everyone who loves science.

Acknowledgments

In the beginning, I would like to greatly appreciate the suggestions and comments on this work by my mentor, Dr. Jung Choi, who provides so much advice and support during my Ph. D program. Furthermore, I greatly appreciate my co-major professor, Dr. Huabei Jiang, who kindly provides so much help and suggestions during the Ph.D. program. Sincerely thank you to my committee members Dr. David Morse, Dr. Mikalai Budzevich, and Dr. Mark Jaroszeski for their kind feedback and help. Thank you very much for the assistance from Dr. Mikalai Budzevich, Dr. Justin Lau, and Epifanio Ruiz from SAIL at Moffitt Cancer Center.

Table of Contents

List of Tables

List of Figures

Abstract

Heart disease, dementia, and stroke are significant public health issues and leading causes of mortality and morbidity worldwide. Abnormalities in blood perfusion and vascular structures are seen in varieties of pathologies, including cerebrovascular diseases like stroke and dementia, hypertension, cardiovascular disease like atherosclerosis, diabetes, peripheral artery disease, and vasculitis, and tumor angiogenesis. Imaging perfusion/vascular abnormalities in these patients often plays a vital role in clinical diagnosis and treatment decisions.

Vascular diseases typically present as macrovascular or microvascular diseases. Microvascular disease (MVD) refers to vascular disease primarily affecting the arterioles, venules, and capillaries in various organs. Furthermore, MVD is widely found in vital organs like the brain, heart, and kidney. The assessment of MVD plays an important role in clinical diagnosis and treatment intervention. While some imaging modalities such as echocardiography, CT, SPECT are widely used to visualize vascular abnormalities, the ability to visualize the microvasculature is often limited or cumbersome. Compared with those imaging techniques, molecular imaging has advantages in visualizing pathology processes at the molecular level to provide early diagnosis like positron emission tomography (PET).

Nuclear blood pool imaging is widely used in the clinical setting for the evaluation of various medical conditions, including impaired cardiac contractility, gastrointestinal hemorrhage, and altered cerebrovascular blood flow by using radiolabeled red blood cells. Nuclear blood perfusion imaging is commonly performed using Technetium-99m-labeled (^{99m}Tc) human erythrocytes (*i.e.*, the “tagged RBC” scan) and gamma camera-based planar scintigraphic

imaging. However, positron emission tomography (PET) provides superior image quality and sensitivity compared to typical clinical planar scintigraphy and single-photon emission computed tomographic (SPECT) imaging platforms. Several PET-based radionuclide agents have been proposed for blood pool imaging, but none have yet to be used widely in the clinical setting. In this body of work, I describe a fast and straightforward procedure for imaging the vasculature of the rat through a combination of a small animal positron emission tomography/computed tomography (PET/CT) scanner and red blood cells (RBC) labeled with widely available and inexpensive PET radiopharmaceutical tracer 2-deoxy-2-(^{18}F)fluoro-D-glucose (^{18}F-FDG). This imaging approach is expected to have significant advantages over traditional ^{99m}Tc -labeled erythrocyte scintigraphic nuclear imaging for a few reasons, including superior spatial resolution and sensitivity. We first demonstrate proof of concept that the entire vascular of an immunodeficient mouse could be visualized using FDG-labeled human red blood cells (RBC).

We showed that FDG-labeled RBC is capable of visual discrimination of the major vessels in the mouse, such as the aorta, vena cava, and jugular veins. In addition, the microvascularity of other organs such as the liver, lungs, and bone marrow could be visualized as well.

In this research, we also investigate the feasibility of this method to semiquantitatively characterize differences in the normal rat myocardial microvasculature between physiologic rest and pharmacologic vasodilatory stress conditions. We also demonstrate the ability of FDG-labeled RBC PET imaging to image the infarcted myocardium in a surgical myocardial infarction rat heart model by using FDG label rat RBC and microPET/CT. Furthermore, we show that FDG-labeled RBC can be used to image the myocardium in a streptozotocin (STZ) induced diabetes rat model under both rest and pharmacologic stress conditions. Compared with normal

age-matched control rats, significant decreases in pharmacologic induced vasodilatory response in the myocardium of the diabetic rats could be detected.

The results provide evidence that this method can be used to visualize differences in myocardial microvascular response to pharmacologic stress conditions in healthy rat diabetic rat myocardium in vivo. This work presents evidence that the 18F-FDG labeling RBC PET image technique may have valuable application for non-invasive PET imaging of various perfusion and vascular disease processes.

Chapter 1: Introduction

1.1 Background

Heart disease, dementia, and stroke, as significant public health issues, are leading causes of mortality and morbidity worldwide [1]. According to the American Heart Association report, the average annual cost of cardiovascular disease and stroke in the USA was about $351.2 billion from 2014 to 2015 [2]. According to the 2018 National Diabetes Statistic Report, approximately 10.5% of the US population has diabetes [3]. Diabetes mellitus is a long-term multifactorial disease associated with a number of vascular complications. It is a significant health problem worldwide and one of the leading causes of death in the United States. Cardiac vascular dysfunction is a severe complication of diabetes and is a significant cause of mobility and mortality in diabetic patients.

Abnormalities in blood perfusion and vascular structures are seen in various pathologies, including cerebrovascular disease like stroke, atherosclerosis, hypertension, and dementia; cardiovascular disease like diabetes, peripheral artery disease, vasculitis, and tumor angiogenesis. Imaging perfusion/vascular abnormalities in these patients often plays an essential role in clinical diagnosis and treatment decisions. Microvascular disease (MVD) is a type of vascular disorder disease phenotypes affecting the small arteries, venules, and capillaries in various organs [4, 5]. MVD is widely found in vital organs like the brain, heart, and kidney [5-9]. Unfortunately, MVD-specific detection methods are limited, making the early diagnosis of MVD challenging. As such robust MVD-specific screening tests would be expected to improve diagnosis and management of MVD.

In the heart, coronary microvascular disease (CVD) can occur with or without obstructive epicardial coronary artery disease, which may be leading to ischemia and angina [10-13]. Catheter-based invasive imaging techniques like coronary flow reserve (CFR) and index of microcirculatory resistance (IMR) are accepted as measures of myocardial blood flow and even microvascular disease, but CFR lacks the ability to distinguish epicardial from microvascular disease and largely limited to invasive coronary angiography [14, 15]. Currently, there are non-invasive modalities like echocardiography, computed tomography (CT), single photon emission tomography (SPECT,) positron emission tomography (PET), and cardiac magnetic resonance (MR) that have been used to understand cardiovascular dysfunction [16]. Microbubble based contrast echocardiography can be used to quantify absolute myocardial blood flow (MBF) in a large epicardial vessel (left anterior descending coronary artery), but these measurements are susceptible to operator dependent differences, require sufficient acoustic window access that may be limited by patient body habitus or comorbidities, and are largely confined to characterizing epicardial artery stenosis-related flow abnormalities [16-18]. Transthoracic Doppler echocardiography has an excellent approach to calculate the coronary flow velocity reserve but with limited use in nonobstructive coronary artery disease [19, 20]. Cardiac magnetic resonance (CMR) and Computed tomography (CT) are also available for non-invasive MVD detection by quantitative MBF measurements [21]. Nevertheless, iodine-based contract CT has high radiation exposure and limited nonobstructive CAD detection ability. Furthermore, iodine signal intensity in CT imaging does not correlate linearly with concentration, and iodinated contrast may cause vasodilation leading to overestimated MBF. Gadolinium signal intensity CMR imaging also does not correlate linearly with concentration; also, these agents diffuse out of the vasculature, requiring more complicated compartment/kinetic modeling [22-24].

PET, as a thriving imaging technology with high tracer sensitivity, has been shown to accurately provide quantitative measurements of myocardial perfusion [21, 25]. PET perfusion tracers Rubidium-82, ^{13}N-NH_3, and ^{15}O-H_2O have good application in absolute quantification of MBF assessment through artery input function (AIF) kinetic modeling. However, these PET perfusion agents have a suboptimal clinical implementation, as they have either restricted availability due to the very short half-life and require more complicated compartment/kinetic modeling [26-28].

1.2 Common Clinical Blood Perfusion and Vascular Imaging Modalities

Gamma camera-based imaging of radiolabeled red blood cells is commonly used for imaging the blood pool in clinical nuclear medicine. For example, ^{99m}Tc-labeled human red blood cells and ^{99m}Tc-labeled human serum albumin blood pool imaging with single photon emission computed tomography (SPECT) or planar scintigraphy have been used to evaluate cardiac function [29-31], gastrointestinal hemorrhage [32], vascular abnormalities [33], and orbital cavernous hemangioma (OCH) [34]. Because PET scanners have superior nuclear tracer sensitivity and image resolution compared to clinical gamma-camera scintigraphy and SPECT scanners [35], the development of a robust PET-based blood pool imaging technique has a significant clinical interest. Multiple PET tracers have been proposed as blood perfusion imaging agents but suffer from certain limitations. For example, 15-oxygen-labeled (^{15}O) $H_2{}^{15}O$, 11-carbon-labeled (^{11}C) ^{11}C-Acetate, 82-rubidium chloride (^{82}Rb), and 13-nitrogen-labeled (^{13}N) $^{13}NH_3$ have been used to investigate myocardial blood flow but are not widely used clinically, as the short radioactive half-life of ^{15}O (122 seconds), ^{11}C (20.334 minutes), ^{13}N (9.97 minutes), and ^{82}Rb (76 seconds) require the presence of a cyclotron in close proximity to the PET scanner or access to an ^{82}Rb generator [36-38]. Due to the positron emitter, 18-fluorine (^{18}F) has a decay

half-life (108 minutes) which is well-suited for clinical imaging, ^{18}F-based tracers are considered attractive for PET imaging, especially given the wide spread prevalence of FDG-specific PET imaging for oncology patients, as well as other ^{18}F-based agents, such as ^{18}F-fluorothymidine (^{18}F-FLT) used for visualizing tumor proliferation[39] .

Computed tomographic angiography (CTA) and magnetic resonance angiography (MRA) are widely used in the clinical setting for the advantages of rapid image acquisition and high resolution blood vessels/tissue delineation, which plays an important role in surgical planning. However, the limitations are that absolute blood flow quantification is not straightforward and parameter dependent, repeat imaging with contrast agent injection is not feasible/practical, and characterization of the microvasculature is limited. Microbubble-enhanced ultrasound has a good application in cardiac, cerebrovascular, and peripheral vascular Doppler imaging to assess both functional and structural cardiac abnormalities like cardiac ejection fraction, cardiac enlargement/wall thickness, cardiac valvular disease, cardiac wall motion abnormalities. However, it has a small acoustic window with limited acoustic access to specific body parts like obesity, gas-filled structures (bowel), overlying bony structures and is also subject to operator-dependent variability. Gamma camera planar blood perfusion and SPECT myocardial perfusion imaging by using Tc-99m labeled red blood cells have wide applications in occult gastrointestinal bleeding, cardiac function, and perfusion imaging for myocardial ischemia/infarction. It has good use in cardiac perfusion imaging, commonly used to detect stress-induced myocardial ischemia. However, the majority of clinically used SPECT scanners have significantly lower sensitivity and spatial resolution compared to positron emission tomography (PET) and is not practical for absolute blood flow measurements. Widespread clinical PET imaging is performed with common PET tracer ^{18}F-Fluorodeoxyglucose (FDG), a

glucose analog that is widely used in oncology detection, cerebral metabolic imaging (stroke, dementia, systemic diseased), and cardiac metabolic imaging.

In this work, we describe the method for labeling human RBC with FDG and washing the FDG-labeled RBC. We also describe the injection of labeled RBC into splenectomized NSG^{TM} immunodeficient mice and subsequent imaging of the mouse vasculature using a small animal microPET/CT platform. Given that the erythrocyte labeling and washing procedure is straightforward and that the FDG leakage rate from labeled erythrocytes is relatively slow (~10% in 46 minutes), we believe this method allows for robust PET imaging of the mouse vasculature. We believe that this imaging technique would be of interest to investigators seeking to visualize the vasculature of immunodeficient mice for other applications. In addition, we speculate that this technique would offer significant advantages over ^{99m}Tc-based nuclear blood pool imaging for the evaluation of occult gastrointestinal bleeding in patients and may be helpful for evaluating other clinical pathologies, including those involving the cerebral and myocardial vasculature.

FDG has a wide application in clinical in quantitative measurements of cardiovascular activity with an ideal half-life. Our research determined that 18F-FDG labeled red blood cells provided a flexible method to image vascular blood perfusion in mice and rats. In this study, we investigated 18F-FDG labeled rat red blood cells (RBC) PET images to visualize the microvascular value under both rest and pharmacologic stress conditions in healthy rats and microvascular abnormalities in infarcted myocardium and diabetic rat model.

1.3 Hypothesis, Research Goal

The overall goal of this work is to develop and characterize a PET-based imaging method in small animal models that can be rapidly transferred to the clinical setting to image

abnormalities in blood perfusion, vascular structure, as well as vascular dysfunction in various organs. This work presents evidence that FDG-labeled RBC PET imaging can be used to visualize the entire vasculature of mouse and rat models, including the microvasculature.

Generally, there is no microvascular dysfunction (MVD) specific imaging technique. In this study, we provide an excellent approach to image the microvascular directly. Furthermore, it was possible to detect the MVD in myocardial dysfunction due to diabetes and infarction.

There are three hypotheses related to the research question. Hypothesis 1: FDG can label human RBCs with high efficiency in a fairly rapid and facile manner, with grossly stable intracellular FDG localization suitable for in vivo imaging of the total vasculature. Hypothesis 2: Pharmacological-induced increases in the rat myocardial and cerebrovascular blood volume can be indirectly visualized as areas of increased intravascular tracer activity with FDG RBC PET imaging, Hypothesis 3: MVD can be semi-quantitatively characterized by FDG RBC PET imaging, including within affected microvasculature in a myocardial infarction rat model, and diabetic induced myocardial MVD.

1.4 Ethics

All experiment procedures were approved by the University of South Florida (USF) Institutional Animal Care and Use Committee (IACUC). All experiments were performed in accordance to federal regulations and USF IACUC principles and procedures. For radiation safety, rats were placed in a clean microisolator, and then the cage was placed within a ventilated cabinet enclosed by 2 inches of lead to allow decay of isotope tracer by 11 half-lives. For the FDG-labeled red blood cells, 18F has a half-life of 110 minutes, so that animals were kept within the shielded cabinet for 21-24 hours. Contaminated bedding was appropriately discarded as radioactive waste. Cages and animals were screened with a gamma Geiger counter to validate

background levels of radioactivity before undergoing euthanasia. The room used for experiments contained all appropriate supplies and equipment for these procedures (e.g., safety goggles with leaded glass, lead-lined solid and liquid waste receptacles, and lead-lined refrigerator/freezer). If an animal died during the experiment, the carcass was bagged and held in the shielded refrigerator for 11 half-lives prior to disposal. Solid and liquid waste disposal was done in accordance with USF Radiation Safety requirements.

Chapter 2: Experiment Design

This chapter was published in Bio-protocol[40]. Permission is included in Appendix A.

2.1 Materials and Reagents

1. 1.8 ml cryovial tube (Thermo Fisher Scientific, Thermo Scientific™, catalog number: 343958)
2. 3.5 ml cryovial tube (Thermo Fisher Scientific, Thermo Scientific™, catalog number: 343958)
3. 15 ml conical tube (Corning, catalog number: 430790)
4. 1 ml sterile syringe (NIPRO Medical Corporation, catalog number: JD+01D2238)
5. 10 cc BD Luer-Lok™ disposable syringe (Thermo Fisher Scientific, catalog number: BD 309604)
6. 15 ml Falcon™ conical centrifuge tube (Thermo Fisher Scientific, catalog number: 14-959-53A)
7. 10 ml and 25 ml Fisherbrand™ Sterile Polystyrene Disposable Serological Pipets (Thermo Fisher Scientific, catalog numbers: 13-676-10F and 13-676-10M)
8. 22 gauge needle (BD™ Needle 1, BD, catalog number: 305155).
9. 26 gauge x ¾” mouse and rat tail vein Monoject IV catheter (Patterson Veterinary, catalog number: 07-836-8403)
10. Parafilm™ M PM996 all purpose laboratory film
11. 200 µl and 1,000 µl TipOne sterile filter pipet tips (USA Scientific, catalog numbers: 1120-8810 and 1122-1830)

12. 0.2 µm Nalgene® bottle top sterile filter unit (Sigma-Aldrich, catalog number: Z370576-12EA)
13. 4-8 weeks old male splenectomized NOD.Cg-*Prkdc*^{scid} *Il2rg*^{tm1Wjl}/SzJ (NSG^{TM}) immunodeficient mice (The Jackson Laboratory, stock number: 005557)
14. 10 ml of human whole blood in standard ACD anticoagulant solution shipped next day (Zen-Bio, Inc, SER-WB10ML-SDS)
15. 1 ml of 2-deoxy-2-(^{18}F)fluoro-D-glucose (^{18}F-FDG) with specific activity calibrated at a minimum of 20 milliCuries/ml at the time of cell labeling (United States Pharmacopeia (USP) grade, Cardinal Health nuclear pharmacy)
16. 0.9% Sodium Chloride Injection USP, 100 ml Fill in 150 ml PAB® (B. Braun, NDC number: 00264-1800-32)
17. 250 ml bottle of IsoThesia (Isoflurane) solution (Henry Schein Animal Health, catalog number: 029405)
18. Sterile de-ionized water
19. NaCl (Sigma-Aldrich, catalog number: S7653-1KG)
20. KCl (Sigma-Aldrich, catalog number: P9333-1KG)
21. K2EDTA dihydrate (Sigma-Aldrich, catalog number: 03660-1KG)
22. EDTA solution 5x (see Recipes)
23. EDTA solution 1x (see Recipes)
24. 1 Unit/ml of heparin sodium salt (see Recipes)
25. Heparin sodium salt (Sigma-Aldrich, catalog number: 375095-100KU)
26. Phosphate Buffered Saline (PBS) solution, pH 7.4 (Thermo Fisher Scientific, catalog number: 10010023)

2.2 Equipment and Software

1. Inveon PET/CT (Siemens Medical Inc., INVEN, catalog number: 138757)
2. Centrifuge 5810 R (Eppendorf, catalog number: 108308)
3. Centrifuge 5810 R (Eppendorf, catalog number: 119548)
4. 200 µl single channel manual pipetter
5. 1,000 µl single channel manual pipetter
6. AtomLab™ 500 dose calibrator (Biodex Medical Systems, Inc)
7. Tissue culture incubator (Sanyo Scientific, catalog number: 133060)
8. Biological safety cabinet (The Baker company, SterilGARD, catalog number: 101951)
9. Rotator platform (Labnet International, Inc GYROMINI)
10. Matlab (Matlab software package, 2018 version)
11. Microsoft Excel program (Microsoft Excel 2010)
12. Inveon PET/CT small animal imaging platform (Siemens Medical Inc., Knoxville, Tennessee)
13. BioVet® (m2m Imaging) physiological monitoring and heating system (m2m imaging Corp. USA. www.m2mimaging.com)

2.3 Procedure

2.3.1 Red Blood Cell (RBC) Preparation

Gently aspirate the whole blood in standard anticoagulant citrate dextrose (ACD) solution (overnight shipping from Zen-Bio, Inc) into a sterile 15 ml conical centrifuge tube by a 10 ml sterile disposable pipet. The original blood sample should have a good quality shown in Figure 2.1.

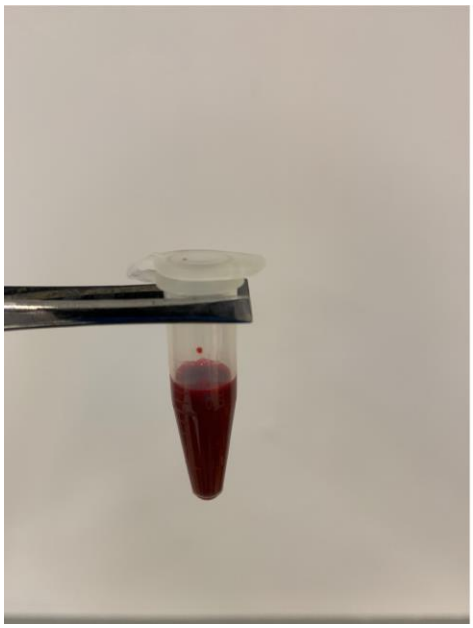

Figure 2.1 The original anti-coagulated blood sample should have no clot and have good fluidity. Reprinted from "Imaging the Vasculature of Immunodeficient Mice Using Positron Emission Tomography/Computed Tomography (PET/CT) and 18F-fluorodeoxyglucose Labeled Human Erythrocytes." by Wang, S. and Choi, J. W. 2019, by Copyright: © 2019 Wang, S. and Choi, J. W, retrieved: https://bio-protocol.org/ 10.21769/BioProtoc.3391., Reprinted with permission.

Blood should be slowly pipetted to minimize mechanical trauma/shear injury to erythrocytes. Centrifuge blood at 1,000 times Earth's gravitational force (1,000 x *g*) 10 min in the desktop centrifuge (no brake) at room temperature.

Slowly aspirate nearly all of the plasma or supernatant from the red blood cell (RBC) fraction using a 1 ml sterile pipet. The plasma should be close to straw-colored or have a slightly reddish tinge, as Figure 2.2. The plasma that has a frankly turbid or significant reddish coloration implies either improper centrifugation or significant pre-existing hemolysis of the original blood sample that may render the sample unsuitable for radiotracer labeling. Slowly transfer 2 ml of pelleted RBCs into 15 ml conical centrifuge tube using 10 ml sterile pipet. Residual plasma and buffy coat should be avoided during erythrocyte aspiration. Add 8 ml of 1x EDTA solution to RBCs. Close cap on the tube and gently invert tube several times to wash cells.

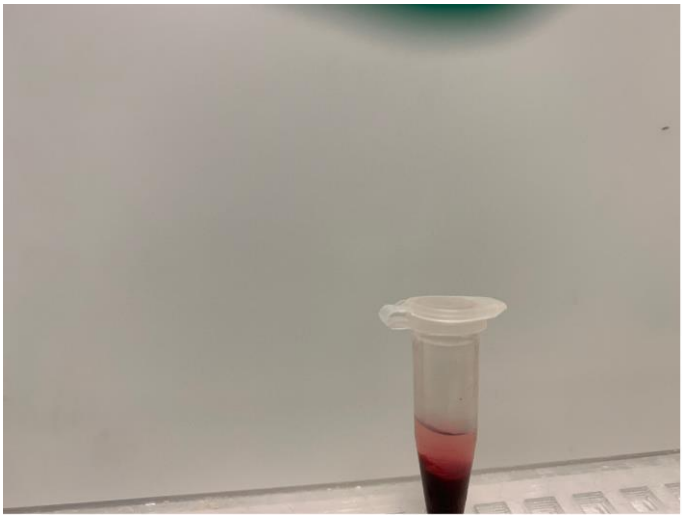

Figure 2.2 The original blood after the first centrifuge step. Ideally, the plasma should be close to straw colored or have a slightly reddish tinge. Reprinted from “Imaging the Vasculature of Immunodeficient Mice Using Positron Emission Tomography/Computed Tomography (PET/CT) and 18F-fluorodeoxyglucose Labeled Human Erythrocytes.” by Wang, S. and Choi, J. W. 2019, by Copyright: © 2019 Wang, S. and Choi, J. W, retrieved: https://bio-protocol.org/ 10.21769/BioProtoc.3391., Reprinted with permission.

Centrifuge 1,000 *x g* 10 min at room temperature, then slowly aspirate the supernatant which is shown in Figure 2.3. with a 10 ml sterile pipet. Rapid supernatant aspiration will disturb the supernatant/RBC interface and result in aspiration of RBCs.

Transfer 250 µl of RBCs with 1,000 into µl pipet tip into 1.8 ml cryovials. Care should be taken to avoid pipetting any residual supernatant.

To each RBC cryovial, add 100 µl 5x EDTA solution and 50 µl sterile de-ionized water (total volume = 400 µl) via a manual pipette.

2.3.2 18F-FDG Labeling of RBC

To maximize the radiolabeling efficiency of RBCs for *in vivo* PET imaging of the vasculature of rat/ mice, the specific activity of USP grade ^{18}F-FDG should be calibrated to at least 20 milliCurie (mCi) per ml at the start of cell labeling.

Add 100 µl ^{18}F-FDG solution to each RBC cryovial (F.V. = 500 µl) behind appropriate radioactivity shielding. Methods for handling radioactive materials for this protocol should follow those established by the radiation safety officer at your institution. Directly count radioactivity in each cryovial using the AtomLab™ dose calibrator (mCi's) and record the time. The amount of activity should be at least 1 mCi of FDG in each vial. Ensure the cap is tightly screwed on the cryovial. Care need be taken when choosing an appropriate vial for FDG RBC labeling, as some cryovials are composed of certain plastics that do not maintain a good seal about the cap when exposed to higher temperatures and can result in local radioactivity leakage/contamination. A thin strip of Parafilm™ can be wrapped around the margins of the cap to ensure no radioactivity leakage from the tube and reduce water loss from the cryovial lumen.

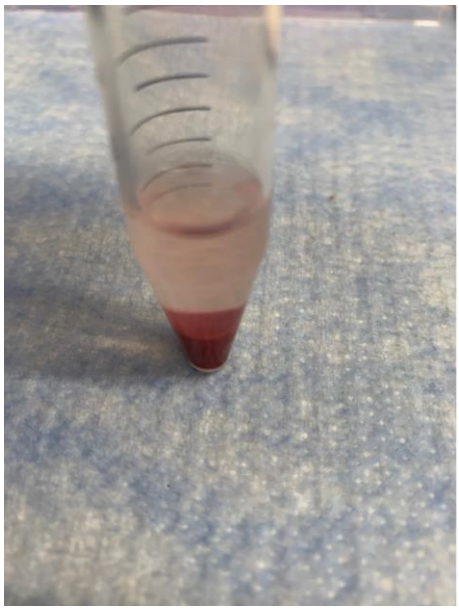

Figure 2.3 The RBCs after washing with 4x volume of 1x EDTA solution. Reprinted from "Imaging the Vasculature of Immunodeficient Mice Using Positron Emission Tomography/Computed Tomography (PET/CT) and 18F-fluorodeoxyglucose Labeled Human Erythrocytes." by Wang, S. and Choi, J. W. 2019, by Copyright: © 2019 Wang, S. and Choi, J. W, retrieved: https://bio-protocol.org/ 10.21769/BioProtoc.3391., Reprinted with permission.

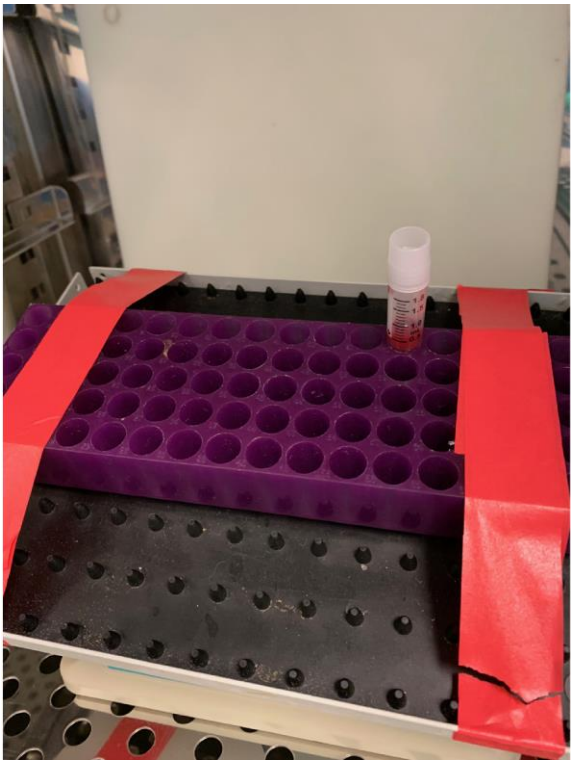

Figure 2.4 RBCs labeled with 100 µl 18F-FDG solution on rotator platform and placed in an upright position in the 37 ℃ incubator. (Reprinted from "Imaging the Vasculature of Immunodeficient Mice Using Positron Emission Tomography/Computed Tomography (PET/CT) and 18F-fluorodeoxyglucose Labeled Human Erythrocytes." by Wang, S. and Choi, J. W. 2019, by Copyright: © 2019 Wang, S. and Choi, J. W, retrieved: https://bio-protocol.org/ 10.21769/BioProtoc.3391., Reprinted with permission.)

Gently finger resuspend RBCs. Place vials in an upright position in a tube rack tied/taped to a rotator platform, as Figure 2.4. Incubate rotating samples in an upright position at 37 °C for 30 min at ≤ 60 RPM. Avoid inverting the tube during rotation, as this likely increases the amount of dried cells adherent to the tube wall.

Centrifuge RBC samples at 1000 *x g* 10 min (no brake) at 4 °C. The present sample is shown in Figure 2.5. Place samples in a ventilated laboratory hood behind appropriate radioactivity shielding and gently transfer the supernatant (about 250 µl) to a 3.5 ml cryovial labeled"SUPE 1 and 2".

Gently resuspend each 250 µl RBC cell pellet in 1 ml 1x EDTA solution via manual pipette. Care should be taken to resuspend cells slowly to minimize pipet-induced mechanical damage/shear injury to cells. Repeat centrifugation of RBC samples at 1,000 *x g* 10 min (no brake) at 4 °C. The centrifuged sample is shown in Figure 2.6.

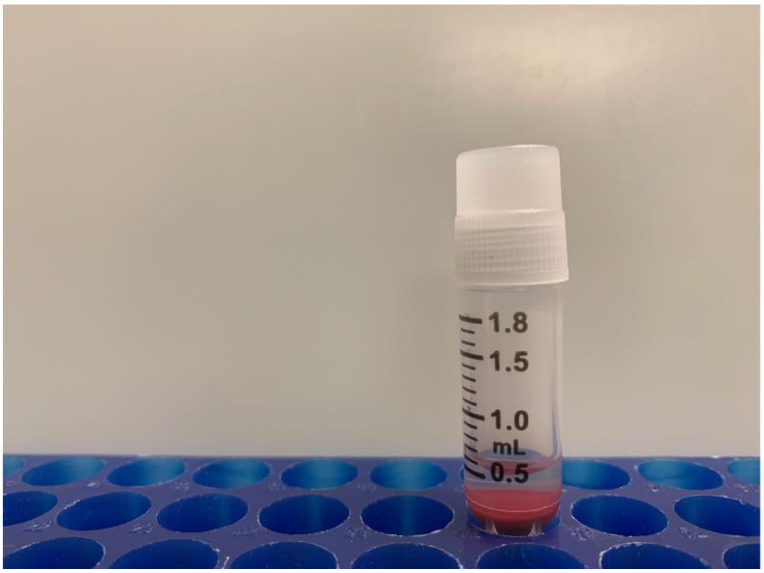

Figure 2.5 The free 18F-FDG fraction (clear upper half of solution) and the precipitated RBCs fraction (red bottom half of the solution). Reprinted from "Imaging the Vasculature of Immunodeficient Mice Using Positron Emission Tomography/Computed Tomography (PET/CT) and 18F-fluorodeoxyglucose Labeled Human Erythrocytes." by Wang, S. and Choi, J. W. 2019, by Copyright: © 2019 Wang, S. and Choi, J. W, retrieved: https://bio-protocol.org/ 10.21769/BioProtoc.3391., Reprinted with permission.

Transfer 2nd supernatant to appropriate "SUPE" tube. Gently resuspend 250 µl RBCs cell pellets again in 1 ml 1x EDTA solution, as described above. Repeat centrifugation of RBC samples at 1,000 *x g* 10 min (no brake) at 4 °C.

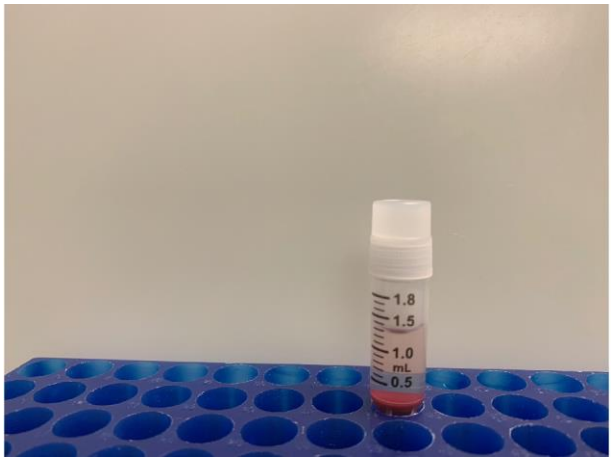

Figure 2.6 Centrifuged 18F-FDG-labeled RBC sample after washing with 1 ml 1x EDTA solution. Reprinted from “Imaging the Vasculature of Immunodeficient Mice Using Positron Emission Tomography/Computed Tomography (PET/CT) and 18F-fluorodeoxyglucose Labeled Human Erythrocytes.” by Wang, S. and Choi, J. W. 2019, by Copyright: © 2019 Wang, S. and Choi, J. W, retrieved: https://bio-protocol.org/ 10.21769/BioProtoc.3391., Reprinted with permission.

Transfer supernatant to appropriate “SUPE” tube. Carefully pipet residual supernatant from the interface with the cell pellet, leaving only a tiny meniscus overlying the pellet.

Directly count SUPE and RBC pellet cryovials using AtomLab detector via dose calibrator (µCurie) and record time. Typical amounts of intracellular radiotracer activity is limited by the total allowable volume of cell solution (250 µl pelleted RBCs) that can be injected into a mouse per day as per our institutional IACUC guidelines, but usually range from ~150 to 300 µCuries, and can be higher depending upon the chosen ^{18}F-FDG specific activity at the start of cell labeling. Gently resuspend the pellet in 250 µl of 1x EDTA solution. The labeling of two RBC samples allows for titration of a larger volume of labeled RBCs, as needed.

Transfer the RBC suspension to a 1 ml syringe using a 22 gauge needle. Any residual clumps of cells should not be aspirated, as these likely represent damaged/coagulated cells. Cells should be slowly aspirated into the syringe lumen to minimize mechanical damage/shear injury

to cells. The radioactivity in the syringe should be measured before and after animal injection to determine net activity injected *in vivo*, as there will be residual activity left in the syringe after injection.

2.3.3 Small Animal PET/CT Imaging

Prepare 4-6 week-old male splenectomized NODSCIDgamma (NSG^{TM}) immunodeficient mice for the experiment.

The mouse can be fasted the night before PET/CT imaging to encourage shifting of mouse metabolic activity from glucose to fatty acids, thus minimizing myocardial uptake of any free FDG in the labeled cell preparation. The mouse/rat can also be placed on a very low carbohydrate diet for this purpose as well, as needed. Draw 500 µl of mouse blood through retro-

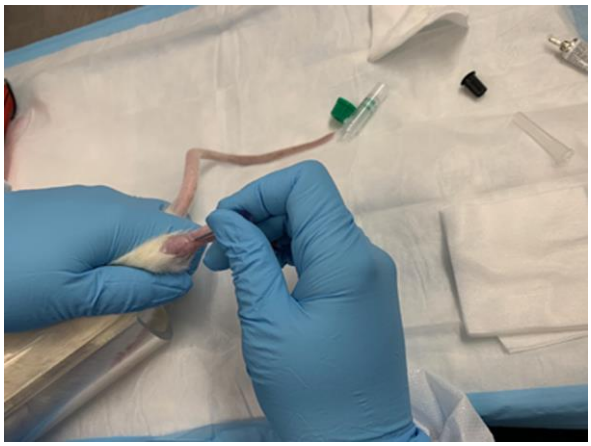

Figure 2.7 Example for drawing blood through rat leg venous. Reprinted from “Imaging the Vasculature of Immunodeficient Mice Using Positron Emission Tomography/Computed Tomography (PET/CT) and 18F-fluorodeoxyglucose Labeled Human Erythrocytes.” by Wang, S. and Choi, J. W. 2019, by Copyright: © 2019 Wang, S. and Choi, J. W, retrieved: https://bio-protocol.org/ 10.21769/BioProtoc.3391., Reprinted with permission.

-orbital venous plexus puncture or other approved venous blood draw at your institution， as seen in the example shown in Figure 2.7. Blood should be collected into the heparinized blood

collection tube. If the blood is drawn too slowly, there is a risk of significant coagulation occurring, rendering the blood sample unsuitable for FDG labeling. Measure blood glucose level with a blood glucose monitor for PET calibration.

Anesthetize the mouse via a nosecone manifold under 2-4% inhalational isoflurane. The lowest level of inhalational isoflurane possible is recommended, as isoflurane may induce vasodilation of the mouse vasculature. Record the level of inhalational isoflurane used per mouse.Warm the mouse tail with either a warm soaked towel to stimulate dilation of the mouse tail veins. Insert a tail vein micro-catheter into one of the dilated mouse tail veins. Flush tail vein catheter with 1 U/ml heparin-PBS solution.

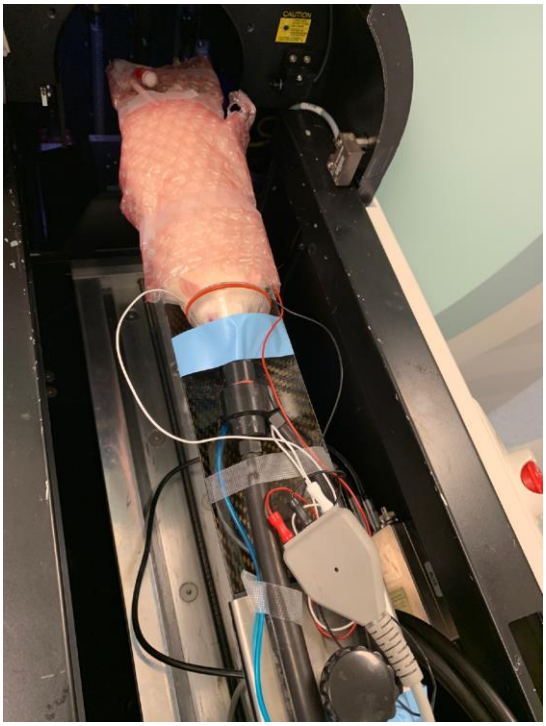

Figure 2.8 Placement of animal in microPET/CT scanner bed for 18F-FDG RBC imaging of the whole body vasculature. Reprinted from “Imaging the Vasculature of Immunodeficient Mice Using Positron Emission Tomography/Computed Tomography (PET/CT) and 18F-fluorodeoxyglucose Labeled Human Erythrocytes.” by Wang, S. and Choi, J. W. 2019, by Copyright: © 2019 Wang, S. and Choi, J. W, retrieved: https://bio-protocol.org/ 10.21769/BioProtoc.3391., Reprinted with permission.

Secure the mouse onto the micro-PET/CT scanner bed under 2-4% inhalational isoflurane anesthesia via nose-cone manifold. The animal can be secured to the micro-PET/CT scanner bed by gently wrapping the animal in bubble packaging to minimize animal movement and preserve body warmth. Care must be taken when wrapping the animal, as tight wrapping may impede animal respiratory motion, as shown in Figure 2.8.

Slowly inject 500 µl of FDG-labeled human erythrocyte suspension into the mouse/rat through the tail vein microcatheter over the course of 1 min to minimize shear injury to cells from passage through the microcatheter lumen. See the example shown in Figure 2.9.

Acquire ECG-gated whole body images of the mouse, followed by CT calibration images. PET/CT image acquisition parameters will depend upon the particular experimental indications and unique imaging platform set up at a given institution; as such, the following is a description of the protocol used at our institution. Place electrocardiogram (ECG) leads on two front limbs and one hind limb of the mouse (ground lead on a rear leg) for ECG gated PET imaging.

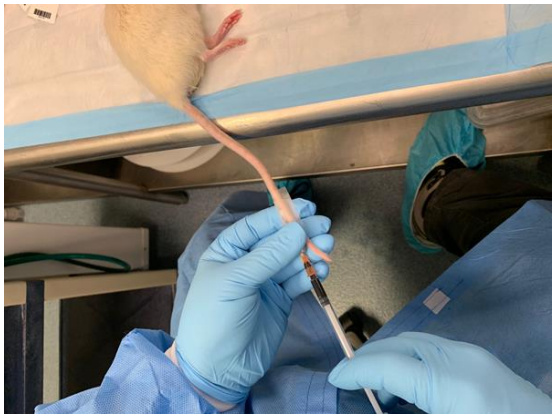

Figure 2.9 Example of injection of FDG-labeled RBC through tail vein microcatheter. Reprinted from “Imaging the Vasculature of Immunodeficient Mice Using Positron Emission Tomography/Computed Tomography (PET/CT) and 18F-fluorodeoxyglucose Labeled Human Erythrocytes.” by Wang, S. and Choi, J. W. 2019, by Copyright: © 2019 Wang, S. and Choi, J. W, retrieved: https://bio-protocol.org/ 10.21769/BioProtoc.3391., Reprinted with permission.

The signals detected by these electrodes are recorded during the 10 minutes time period by BioVet® (m2m Imaging) physiological monitoring and heating system. Set the threshold for TTL cardiac gating signals in a rising mode of R-wave peak. Reconstruct the PET list-mode data using 3D-OSEM iterative algorithm with four iterations and eight subsets, with a final image volume of 256 x 256 x 256 voxels. Set effective voxel effective dimensions at 1.4 x 1.4 x 1.4 mm. For each animal, there are three data sets: dynamic 3D PET reconstruction with 30 frames; standard 3-dimensional (3D) PET reconstruction, resulting in a motion–time average 3D PET image; and the phase-based 4-dimensional (regular 3-dimensional plus time, 4D) PET cardiac reconstruction, with four cardiac gate binning. Please see Figure 2.10. and 2.11. In all cases, CT attenuation correction is applied to the PET images (Choi *et al*., 2019).

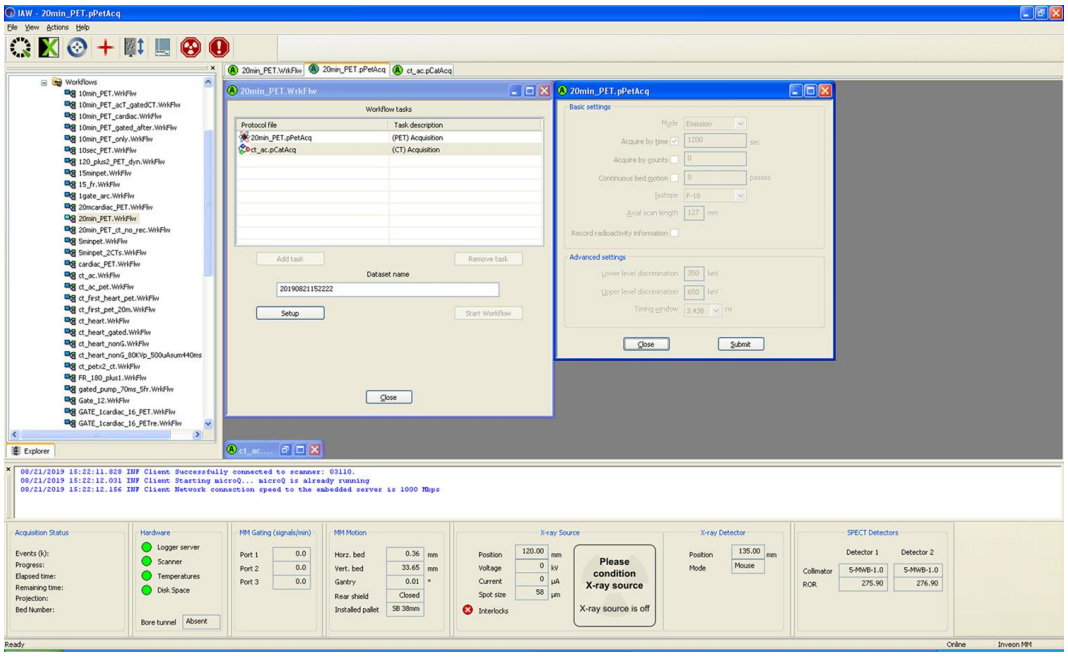

Figure 2.10 Example for microPET acquisition set up. Reprinted from "Imaging the Vasculature of Immunodeficient Mice Using Positron Emission Tomography/Computed Tomography (PET/CT) and 18F-fluorodeoxyglucose Labeled Human Erythrocytes." by Wang, S. and Choi, J. W. 2019, by Copyright: © 2019 Wang, S. and Choi, J. W, retrieved: https://bio-protocol.org/ 10.21769/BioProtoc.3391., Reprinted with permission.

2.4 Data Analysis

2.4.1 Micro-PET/CT Analysis

PET/CT image processing/analysis parameters will depend upon the particular experimental indications and unique imaging platform set up at a given institution; as such, the following is a description of the protocol used at our institution. Analyze the whole body PET images of the mouse using Inveon Workstation Software (Siemens Medical Inc., Knoxville, Tennessee). Select the vendor software-supplied Patlak compartment plot option for kinetic modeling. For 3D PET and 4D PET data sets, manually select multiple volumes of interest (VOI) based on corresponding CT images for the following organs (as needed): heart, leg muscle, liver, kidney, and brain. Voxel activities are represented in standardized uptake values (SUV). Plot dynamic activity curves for VOIs using dynamic 3D PET data set for each animal.

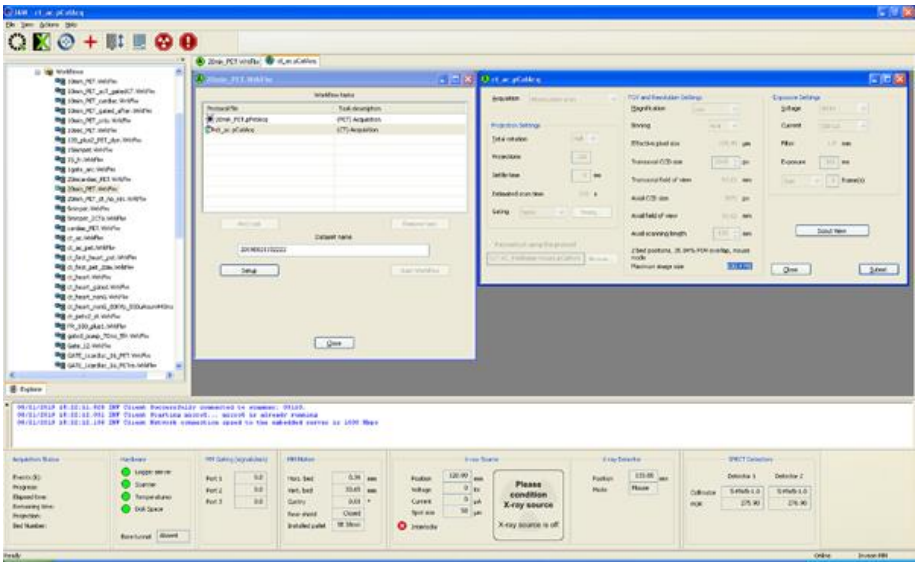

Figure 2.11 Example for microCT acquisition set up using Siemens Inveon platform. Reprinted from "Imaging the Vasculature of Immunodeficient Mice Using Positron Emission Tomography/Computed Tomography (PET/CT) and 18F-fluorodeoxyglucose Labeled Human Erythrocytes." by Wang, S. and Choi, J. W. 2019, by Copyright: © 2019 Wang, S. and Choi, J. W, retrieved: https://bio-protocol.org/ 10.21769/BioProtoc.3391., Reprinted with permission.

The 4D PET data are used for defining cardiac function. First, segment the heart on CT images based on anatomical features, then transfer the segmented volume (cardiac PET VOI) for image co-registration, as seen with the example shown in Figure 2.12. Images are represented as maximum intensity projection (MIP) reconstructions of the source data. ECG-guided binning of PET MIP images can be performed to obtain pseudo-dynamic images of mouse cardiac contractility.

2.4.2 Labeling Efficiency Calculation

Labeling efficiency = (radioactivity dose of RBC pellet)/(radioactivity dose of SUPE + radioactivity dose of RBC pellet)

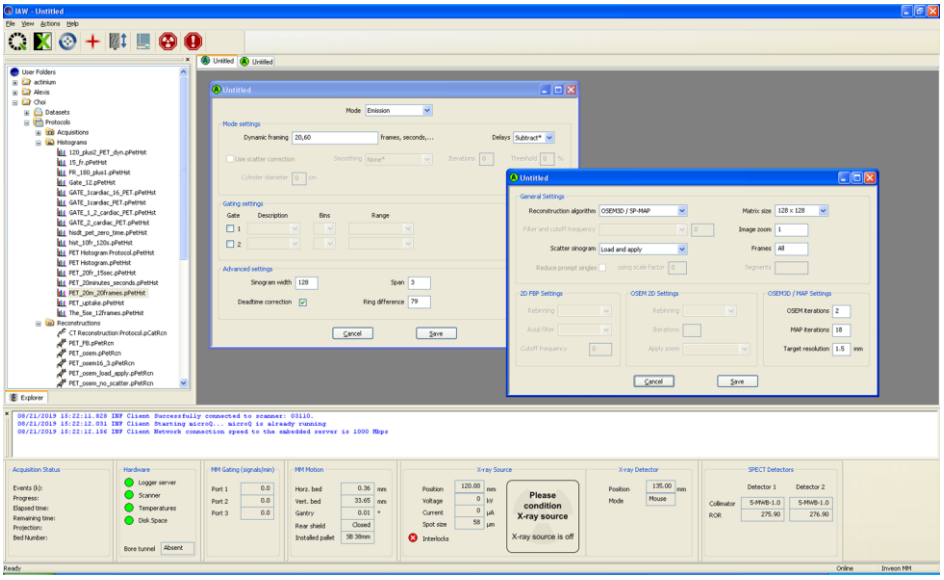

Figure 2.12 Example of basic parameter setup for microPET/CT reconstruction on Siemens Inveon workstation. Reprinted from “Imaging the Vasculature of Immunodeficient Mice Using Positron Emission Tomography/Computed Tomography (PET/CT) and 18F-fluorodeoxyglucose Labeled Human Erythrocytes.” by Wang, S. and Choi, J. W. 2019, by Copyright: © 2019 Wang, S. and Choi, J. W, retrieved: https://bio-protocol.org/ 10.21769/BioProtoc.3391., Reprinted with permission.

2.5 Recipes

1. Filter sterilized 100 ml 5x EDTA solution

   700 mM NaCl

   20 mM KCl

   12.5 mM K_2EDTA dihydrate. Add sterile de-ionized water to a final volume of 100 ml

   Pass final solution through 0.2 micrometers (µm) Nalgene bottle top sterile filter unit

2. 100ml 1x EDTA solution

   20 ml of filter sterilized 5x EDTA solution

   80 ml of sterile di-ionized water

   Pass final solution through 0.2 micrometer (µm) Nalgene bottle top sterile filter unit

3. 1 Unit/ml of heparin-PBS solution

   Heparin sodium salt dissolved in sterile Phosphate Buffered Saline (PBS) solution, pH 7.4.

Chapter 3: Pharmacological-induced Increases in Myocardial and Cerebral Blood Value Measurement

3.1 Research Purpose

Compared to dominant clinical planar scintigraphy and single-photon emission computed tomographic (SPECT) blood perfusion imaging platforms. PET has significant advantages in imaging quality and resolution sensitivities. We seek to show that FDG-labeled red blood cells can be used to image the vasculature in mice and rats and measure the rat myocardial and cerebral blood volume before and after pharmaceutical stress drug-induced vascular dilation. This study presents a novel imaging technique for imaging heart muscle and cerebral vascularity. The purpose of this chapter study is to determine if the FDG-labeled rat red blood cells can also be used to measurement changes in blood volume to the rat heart and the brain after administration of the pharmaceutical drug regadenoson and acetazolamide.

Regadenoson is a selective short-acting adenosine A2A receptor agonist that stimulates vasodilation of the coronary arteries [41]. This drug is widely used in the clinical setting to induce pharmacologic "stress" of the heart in patients undergoing SPECT myocardial perfusion imaging. In this work, this drug is to be administered via the tail vein catheter in order to determine if FDG-labeled cells can detect the increase in rat myocardial vascular volume after administration of this drug. Detecting small changes to the volume of the myocardium with this method could potentially be used to diagnose different types of cardiac vascular dysfunction, including infarction and diabetic-induced cardiomyopathy. Aminophylline is an adenosine receptor antagonist that is administered to rats to reverse the vasodilatory effects of the drug

Regadenoson [42]. This will allow PET imaging of the rats under initial pharmacologic stress (Regadenoson) imaging, reversal of Regadenoson effects with aminophylline, followed by "rest" imaging. Acetazolamide is known to dilate brain vessels, resulting in increased blood perfusion to the brain[43]. Detecting small changes in blood volume to the brain with this technique could potentially be used to diagnose different types of dementia, including Alzheimer's disease.

For purposes of improving the myocardial chamber and ventricular wall segmentation, the same protocol for imaging the myocardium and blood pool will be used as described in the original protocol, but with the additional injection of 0.8 ml's (80 mg) of 15 nm Aurovist gold nanoparticles prior to FDG-labeled RBC injection. The gold nanoparticles allow for more accurate volumetric measurement of the left ventricular muscle needed to segmentation FDG RBC PET activity in the myocardial.

3.2 Experiment Procedure

3.2.1 Stress and Rest Myocardial Blood Perfusion Imaging Process

Secure the rat onto the micro-PET/CT scanner bed under 2-4% inhalational isoflurane anesthesia via a nose-cone manifold. The animal can be secured to the micro-PET/CT scanner bed by gently wrapping the animal in bubble packaging to minimize animal movement and preserve body warmth.

The ability to measure myocardial perfusion with FDG-RBC PET imaging would potentially allow for the detection of myocardial microvascular disease. The procedure is as follows: Non-lethal rat blood phlebotomy samples were collected via a saphenous vein or subclavian vein after anesthesia into an anticoagulant (heparin) container. Alternatively, retro-orbital phlebotomy can be performed, as initial phlebotomy experiences with these rats using the saphenous vein approach may sometimes be difficult.

Rat red blood cells are purified and then labeled with the PET tracer FDG. A tail vein catheter is placed into the rat under anesthesia. FDG-labeled rat red blood cells are then injected through a tail vein catheter, then injected with the coronary vasodilator drug Regadenoson (Sigma Aldrich, St. Louis, MO) (25 μg/kg in 100 μl 1x EDTA solution) to induce pharmacologic stress of the heart, and then undergo microPET imaging for 15-20 minutes and CT 5-10 minutes. After that, the rat was injected with Aminophylline (Sigma Aldrich, St. Louis, MO) (40 mg/kg in 200 μl DI water) to reverse the myocardium vasodilation. Following by 15-20 minutes microPET imaging and 5-10 minutes of CT imaging.

After a sufficient number of imaging experiments have been completed to obtain statistically significant results, the rats will be euthanatized under inhalational anesthesia.

3.2.2 Stress and Rest Cerebral Blood Perfusion PET/CT Imaging Process

The design for the procedure to image rat cerebral blood perfusion is very similar to the original protocol; it is as follows: Non-lethal rat blood phlebotomy samples collected as according to the original protocol or collected via subclavian vein after rat got anesthesia. Rat red blood cells are purified and then labeled with the PET tracer FDG. A tail vein catheter is placed into the anesthetized rat. FDG-labeled rat red blood cells are then injected through the tail vein catheter. Then undergo microPET imaging for 15-20 minutes and CT 5 -10 minutes. After that, the rat was injected with the pharmacological vasodilation drug Acetazolamide (Sigma Aldrich, St. Louis, MO) (100mg/kg in 200 μl Dimethyl sulfoxide (DMSO) buffer) to induce cerebral vasodilation. The vasodilator acetazolamide is then injected through the catheter, and an additional microPET imaging for 15-20 minutes and CT 5 -10 minutes is performed to image the rat brain. After a sufficient number of imaging experiments have been completed to obtain statistically significant results, the rats will be euthanatized under inhalational anesthesia.

3.2.3 Gold Nanoparticle Enhanced Contrast Myocardial CT Imaging

A tail vein microcatheter is placed into the anesthetized rat. And then, secure the rat onto the micro-PET/CT scanner bed under 2-4% inhalational isoflurane anesthesia via a nose-cone manifold. Injection of 0.4 ml's (80 mg) of 15 nm Aurovist gold nanoparticles (Sigma Aldrich, St. Louis, MO) through the microcatheter prior to CT and then undergo CT scanning 5-15 minutes.

3.2.4 RBC Damage Measurement by Flow Cytometry

To measure the degree of mechanical RBC membrane damage induced by multiple washing and centrifugation steps in the FDG labeling RBC process. The RBC samples were evaluated by Annexin V-PE and Calcein-AM double-labeling flow cytometric analysis, acetoxymethyl ester of calcein (Calcein-AM) (Sigma Aldrich, St. Louis, MO), a fluorescein dye maker for cell membrane integrity and viability[44]. Annexin-V-phycoerythrin (Annexin V-PE) (Sigma Aldrich, St. Louis, MO) is an early eryptosis fluorescein marker [45].

Remove supernatant and buffy coat after centrifuging the blood at 1000 x *g* for 10 minutes. Re-suspend the RBC pellet in 4 x value of 1x EDTA solution and spin it 1000 x *g* for 10 minutes, and then remove the supernatant. The blood was divided into three groups, each group experiment repeated at least three times.

FDG labeling RBC test group measurement: after mock the FDG labeling procedure. Using the equivalent value of 1 x EDTA buffer solution for FDG. Incubate the blood at 37°C for 30 minutes, and then wash with 4 x value of 1 x EDTA solution for two times and centrifuge three times. Dilute approximate 4 x 10^5 RBC in 1 x PBS buffer sample to a volume of 80 µl. Add 80 µM Calcein AM dye, 10 µl Annexin V-PE and 400 µl 1x Annexin V bind buffer. Incubate the samples at 37°C for 90 minutes in the dark. Positive and negative control group: dilute approximate 4 x 10^5 unperturbed RBC in 1 x PBS buffer sample to volume of 80 µl. Add 80 µM

Calcein AM dye, 10 µl Annexin V-PE and 400 µl 1x Annexin V bind buffer. Incubate the sample in 37°C for 90 minutes in the dark as the positive control group. Dilute approximate 4 x 10^5 unperturbed RBC in 1 x PBS buffer sample to volume of 70 µl. Add 80 µM Calcein AM dye, 10 µl Annexin V-PE, 10 µl 20mM calcium chloride buffer solution, and 400 µl 1x Annexin V binding buffer. Incubate the sample in 37°C for 90 minutes in the dark as the negative control group. Transfer the blood samples to flow cytometry tube and evaluated with flow cytometric analysis.

3.2.5 FDG Labeling RBC Release Fraction Measurement

In order to evaluate the FDG release ratio from labeled RBC, one-day-old human blood was labeled with FDG using the previously labeling procedure. The washed 250 µl RBC samples were incubated with 375 µl plasma in 37°C for 30, 60, and 90 minutes. Centrifuge the samples at 1000 x *g* for 10 minutes after accurate incubation, and directly count the radioactivity dose of supernatant and RBC pellet using AtamLab detector via dose calibrator. The release fraction= radioactivity dose of supernatant / (radioactivity dose of supernatant + radioactivity dose of RBC pellet). Sample activity counting was made approximately 16 minutes plus the incubation period after the start of the plasma incubation.

3.3 Results

Myocardial vascular imaging: FDG-RBC PET/CT imaging allows for the detection of blood perfusion in rat body as Figure 3.1 & 3.3 shows a 3-D view of blood perfusion in rat a portion of the rat body by FDG RBC PET/CT image. The vascularity in various organs, including the heart and the brain, and the jugular veins, arteries, brain veins are all visualized in Figure 3.1; the low-right showed the 3-D fused maximum intensity projection (MIP). The differences were calculated by digital subtraction of the stress and rest conditions images after

segmentation of the myocardium as Figure 3.8, coronal and axial segmentation of normal rat myocardial on FDG RBC PET/CT images for stress and rest conditions, separately. After digital subtraction of the stress and rest slices as Figure 3.9, the increased value in myocardial vasculature can be visualized by FDG RBC PET imaging. What is more, the activities in rest/stress conditions of the heart can be quantified as Figure 3.10 & 3.11 & Table 3.1. We were able to detect a relative regadenoson-dependent increase in LV intramyocardial vessel volume with a mean pharmacologic stress-related increase in volume of 52.3% ± 11.3% (Bq/ml) (n=5). The difference in intramyocardial vascular volume (stress vs. rest) was statistically significant (two- tailed Wilcoxon signed rank test: $U = 0 \leq 2$, $\alpha = 0.05$, $n = 5$).

Cerebrovascular imaging: the cerebral vasculature is imaged as Figure 3.2, 3-D view by RBC microPET/CT image zoom in rat brain. Top-left is the axial orientation view of the rat brain, and the top-right is the sagittal orientation view of the rat brain, the bottom-left is the coronal orientation of the rat brain, and the bottom-right fused MIP 3-D view of the rat brain. The differences were calculated by digital subtraction of the stress and rest conditions images after segmentation of the brain as Figure 3.4, for stress and rest conditions, separately. After that, digital subtraction of the stress and rest slices as Figure 3.5, the increased value in cerebral vascular volume is indirectly visualized by FDG RBC PET imaging. What is more, the activities in rest/stress conditions of the brain can be quantified as Figure 3.6 & 3.7 & Table 3.1. After administration of acetazolamide, there is a significant relative vasodilator-induced increase in the total cerebrovascular volume of 72.2% ± 14.7% (n=6). The difference in stress vs. rest cerebrovascular volume was statistically significant (two-tailed Wilcoxon signed rank test: $U = 0 \leq 2$, $\alpha = 0.05$, $n = 6$).

Gold nanoparticle enhanced contrast myocardial CT imaging: the gold nanoparticles allow for more accurate volumetric measurement of the left ventricular muscle needed to quantify FDG RBC PET activity in the myocardial vasculature, as shown in Figure 3.12. The myocardial chamber and ventricular wall are all visualized and easily segmented under the gold nanoparticles enhanced CT. However, PET imaging is sufficient for myocardium and ventricular chamber segmentation. The gold nanoparticles enhanced CT was initially pursued to improve with the myocardial chamber and ventricular wall segmentation but was later not deemed necessary.

RBC membrane damage assessment by flow cytometry: as Figure 3.13 flow cytometry for RBC damage measurement results showed, the FDG labeling RBC procedure induced minimum damage to the RBC. The labeling procedure test group has a very close calcein AM positive percentage of about 98 % compared with the untreated group about 97% percent calcein AM positive result. It indicates that this labeling method is safe and straightforward with minimum FDG damage. Unlike the C：CaCl2-treat group, which has 2.17% calcein AM positive and 82.03% annexin V-PE positive.

FDG labeling RBC release fraction measurement: the FDG labeling RBC release fraction measurement is shown in Figure 3.14. It has about 10% release fraction after 46 minutes at the start point, and it is about 1% percent leakage which is correlated with free FDG residual in RBC during the pipe removing supernatant procedure. During the 20 minutes of PET scanning. It has about 5% leakage.

3.4 Figures and Tables

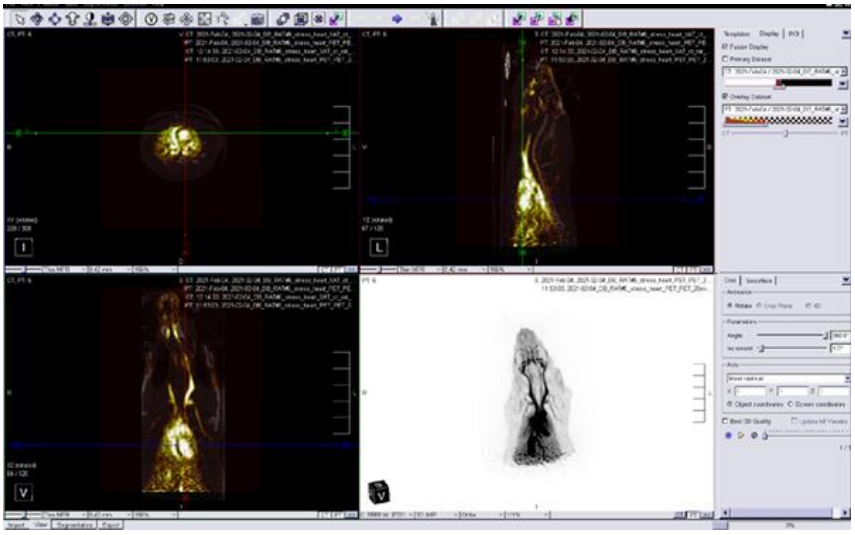

Figure 3.1 3-D view of blood perfusion by RBC microPET/CT image zoom in rat heart. Top-left is the axial orientation view of the rat heart, and the top-right is a sagittal orientation view of the rat heart. Bottom-left is the coronal orientation of the rat heart. Bottom-right is the fused MIP 3-D view of the rat heart.

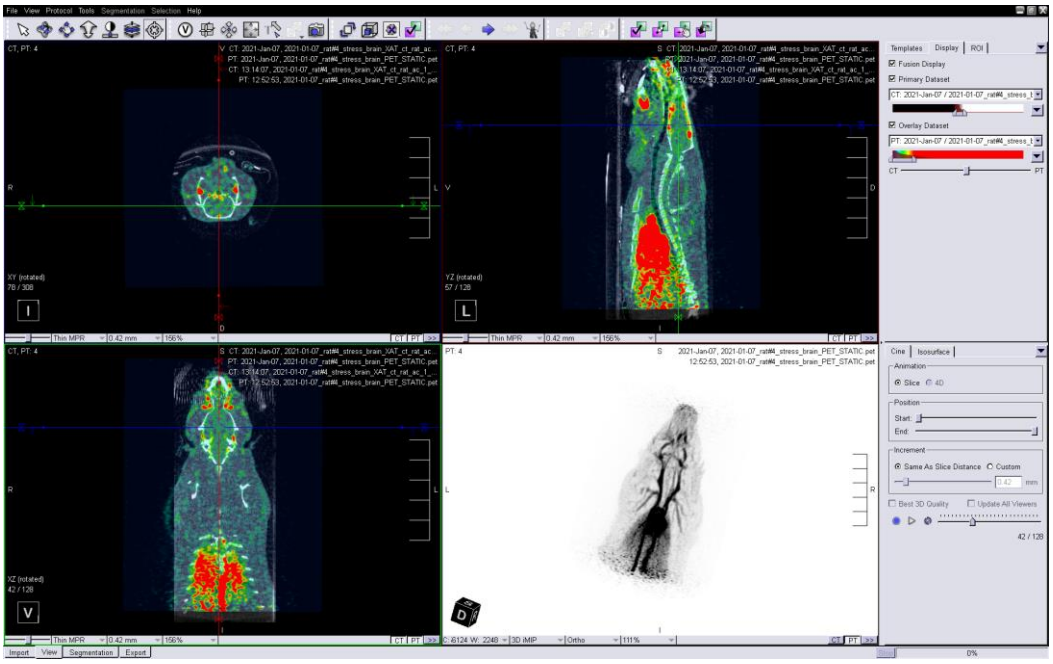

Figure 3.2 3-D view of blood perfusion by RBC microPET/CT image zoom in rat brain. Top-left is the axial orientation view of the rat brain, and the top-right is the sagittal orientation view of the rat brain, the bottom-left is the coronal orientation of the rat brain, and the bottom-right fused MIP 3-D view of the rat brain.

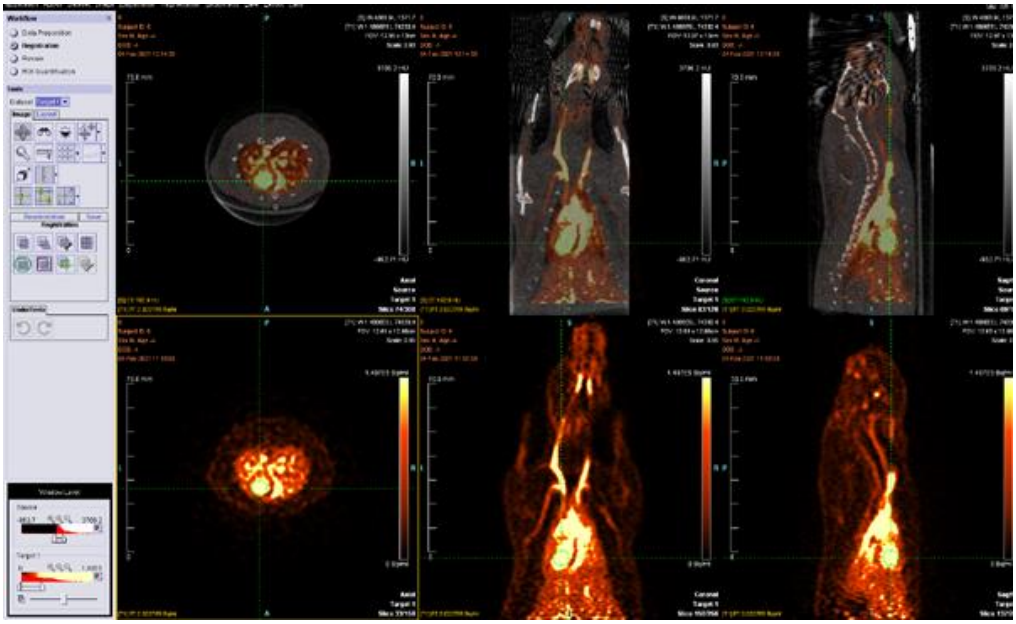

Figure 3.3 2-D visualize of blood perfusion in rat body 20 frames by RBC micoPET/CT.

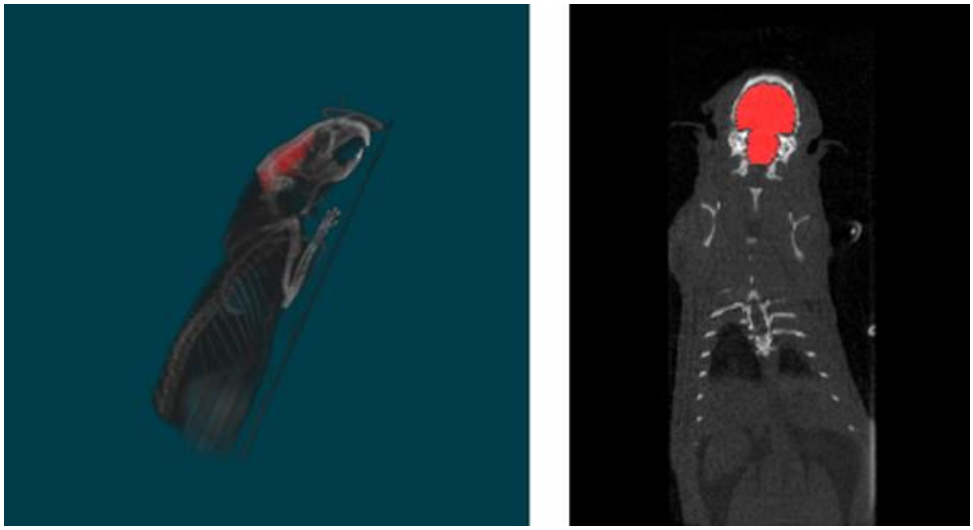

Figure 3.4 Segmentation of rat brain. Left: fused 3-D view of rat brain segmentation, right: coronal view of rat brain segmentation.

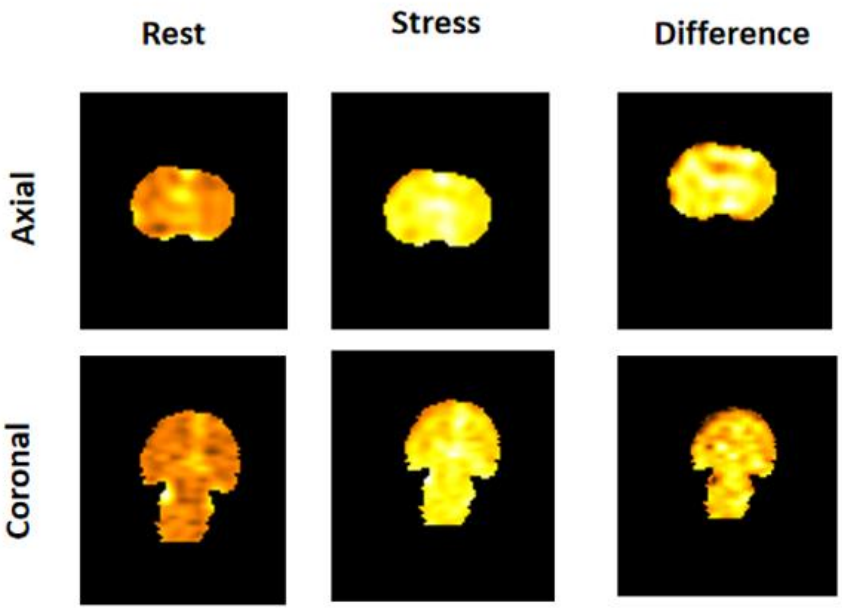

Figure 3.5 Digital subtraction of stress rest condition rat brain view.

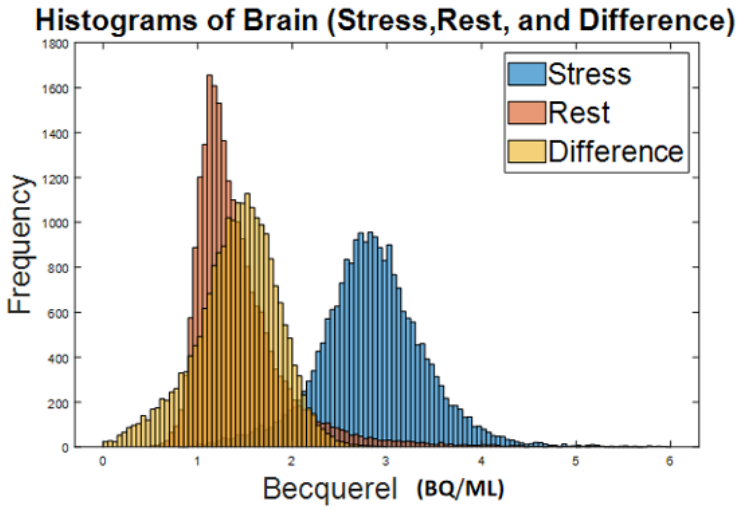

Figure 3.6 Becquerel histograms of rat brain.

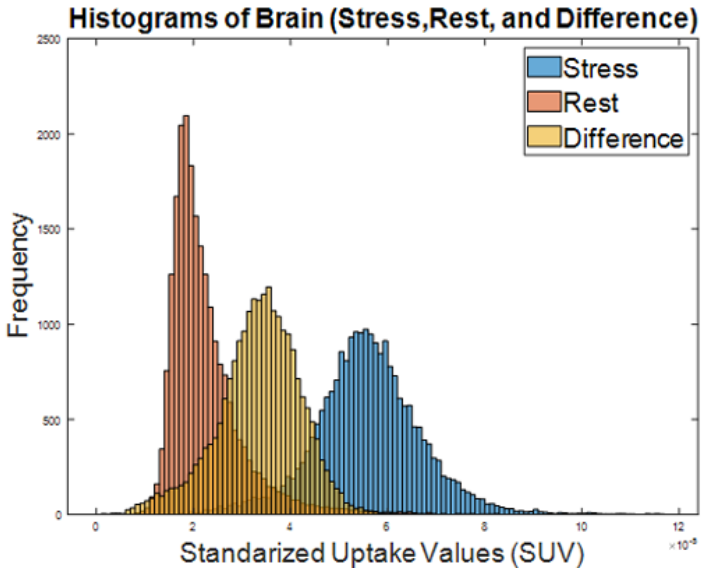

Figure 3.7 Standardized uptake values (SUV) histograms of rat brain.

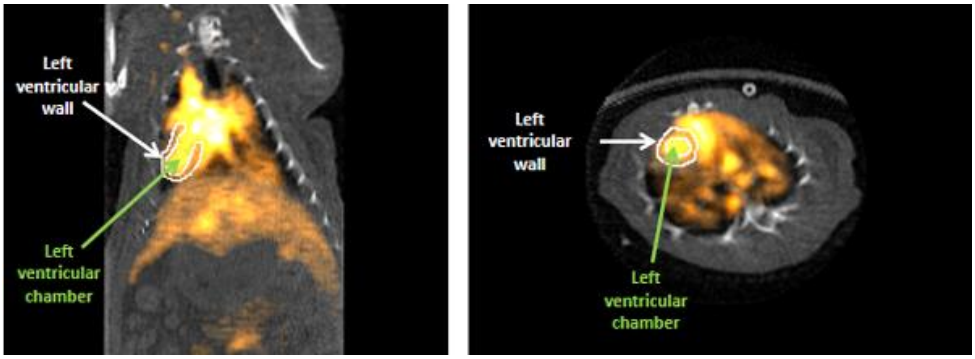

Figure 3.8 Coronal segmentation of normal rat myocardial on FDG RBC PET/CT images.

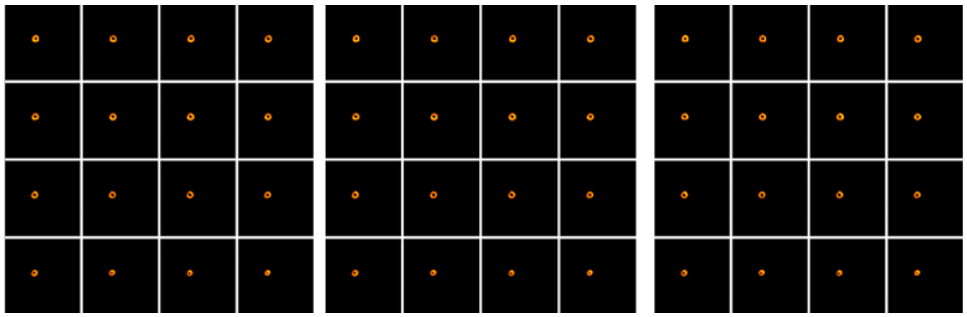

Figure 3.9 Stress-rest myocardium short axial view the short axis view of rat left ventricular wall. Left stress condition, middle, after-stress (rest), right, the difference after subtraction stress and rest images.

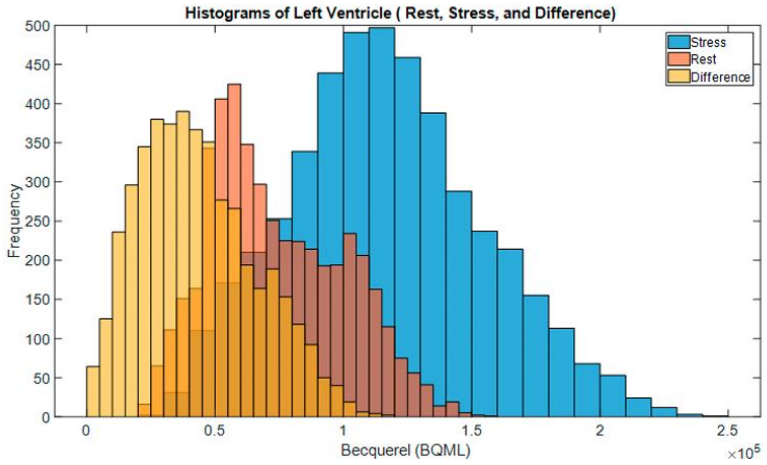

Figure 3.10 Becquerel histograms of rat heart.

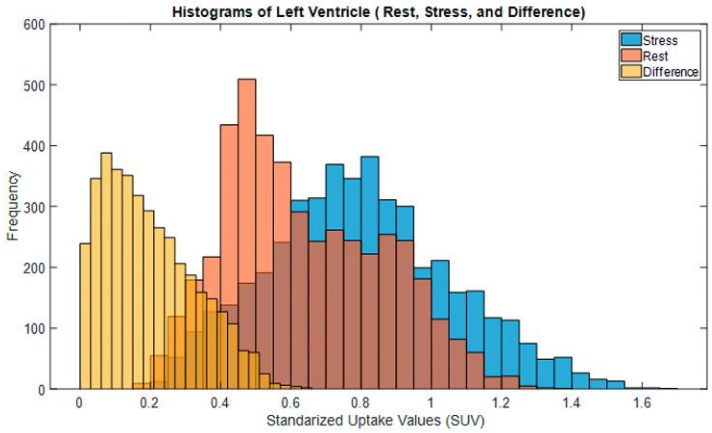

Figure 3.11 Standardized uptake values (SUV) histograms of the rat myocardial.

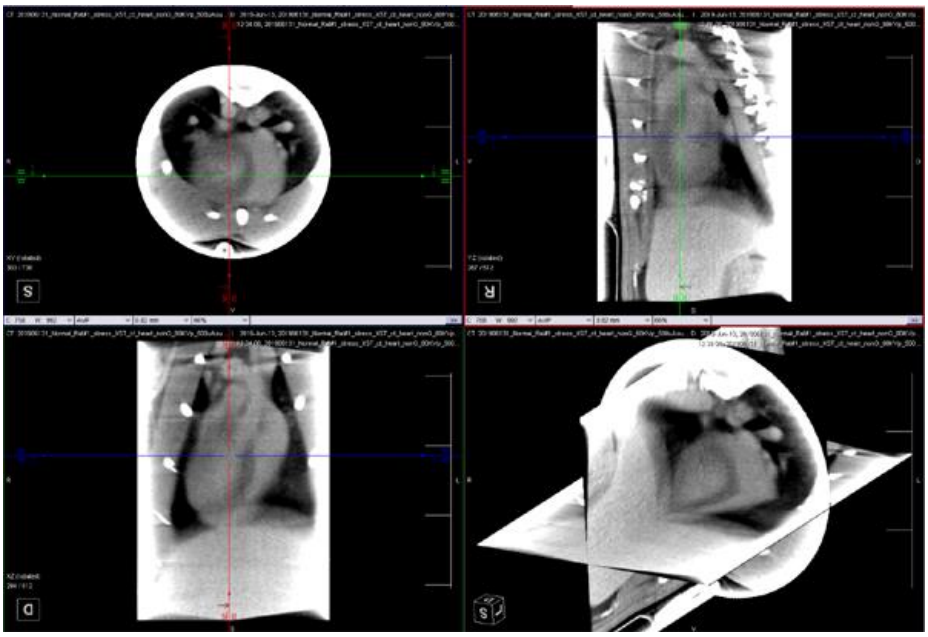

Figure 3.12 Gold nano-particle contrast microCT imaging of normal rat heart. Top-left is the axial orientation view of the rat heart, and the top-right is the sagittal orientation view of the rat heart, the bottom-left is the coronal orientation of the rat heart, the bottom-right is the fused 3-D view of the rat heart.

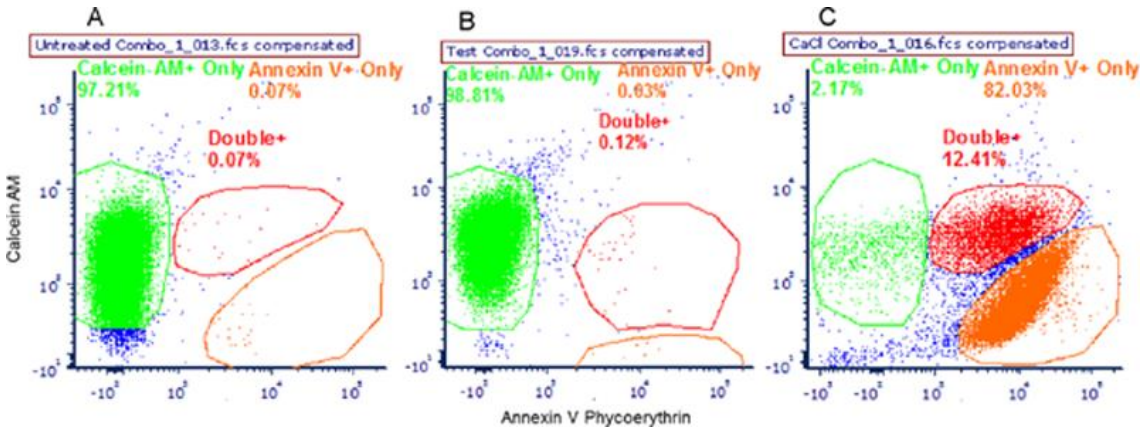

Figure 3.13 Flow cytometric analysis of levels of rat RBC apoptosis induction and RBC plasma membrane damage after mock FDG labeling procedure. A： negative control group without any treatment to RBC, B：FDG RBC test group with all the labeling procedure, C：CaCl2-treat group which induced much damage to cells. Reprinted from “In vivo positron emission tomographic blood pool imaging in an immunodeficient mouse model using 18F-fluorodeoxyglucose labeled human erythrocytes.” by Choi JW, Budzevich M, Wang S, Gage K, Estrella V, Gillies RJ (2019), PLoS ONE 14(1). Copyright: © 2019 Choi et al. Retrieved: https://doi.org/10.1371/journal.pone.0211012, Reprinted with permission.

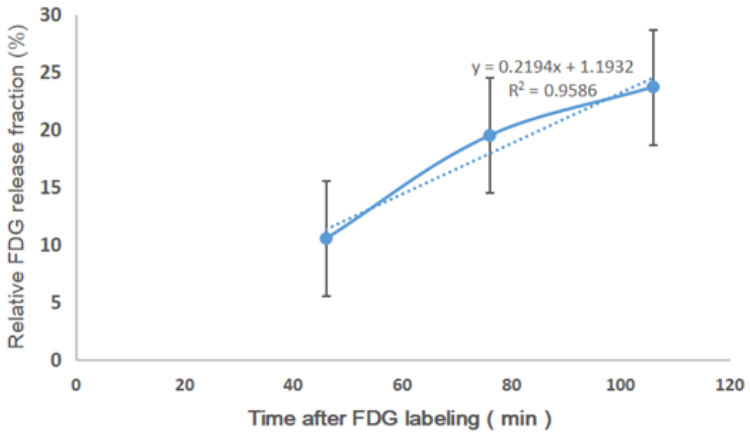

Figure 3.14 FDG labeling RBC release fraction measurement. Reprinted from "In vivo positron emission tomographic blood pool imaging in an immunodeficient mouse model using 18F-fluorodeoxyglucose labeled human erythrocytes." by Choi JW, Budzevich M, Wang S, Gage K, Estrella V, Gillies RJ (2019), PLoS ONE 14(1). Copyright: © 2019 Choi et al. Retrieved: https://doi.org/10.1371/journal.pone.0211012, Reprinted with permission.

Table 3.1 Measurement of the tracer activity intensity (BQ/ML) and standardized uptake value (SUV) in both rest and stress conditions of the heart FDG PET imaging

Heart	Mean	S.E.	SUV	S.E
Rest	29735.66	8326.20	1.00	0.28
Stress	32177.48	9511.53	1.28	0.38
Difference	5186.25	6793.77	0.33	0.31

Table 3.2 Measurement of the tracer activity intensity (BQ/ML) and standardized uptake value (SUV) in both rest and stress conditions of the brain FDG PET imaging

Brain	Mean	S.E.	SUV	S.E
Rest	8739.55	3297.56	0.17	0.06
Stress	20086.95	4040.07	0.33	0.07
Difference	11368.22	4297.09	0.16	0.07

3.5 Discussion

The work in this chapter demonstrates the feasibility of 18F-FDG labeling RBC as a novel perfusion tracer for evaluation of total myocardial and cerebral microvascular value under both rest and pharmacologic stress conditions. As the rat myocardium is 90-95% microvascular

in volume, we demonstrate through subtraction imaging FDG RBC PET's ability to image the myocardial microvasculature under both rest and pharmacologic stress conditions. We measured the myocardial microvascular value using FDG RBC PET imaging and subtraction of stress and rest conditions images. The total myocardial vascular activity was imaged by FDG RBC PET images, and the difference between stress and rest conditions was indirectly visualized after subtraction of stress and rest conditions images. It has adequate image quality, allows for quantitative evaluation of the total myocardial vasculature under stress and rest conditions.

This work shows that FDG RBCs PET imaging can detect changes in the myocardial and cerebral vasculature after pharmacological drug-induced vasodilation. We believe that FDG RBCs PET imaging would also be capable of quantitative myocardial blood flow measurements on modern clinical PET/CT scanners.

In this work, we find that FDG labeled RBC activity remains largely intravascular in location during the acquisition time, given possible slow FDG leak from RBC; thus, it should be theoretically feasible to use one compartmental kinetic modeling for clinical applications. Due to the small animal PET/CT scanner limitations, the smallest temporal resolution possible with the Siemens Inveon microPET/CT scanner is one second, which is unfortunately too slow to accurately use an arterial input function (AIF) myocardium to quantify the absolute myocardial blood flow (MBF). However, it is not expected to be an issue for clinical application due to the adequate spatial and temporal resolution of modern PET/CT scanners.

Chapter 4: Myocardial Microvascular Dysfunction Measurement in Rats with Myocardial Infarction

4.1 Research Purpose and Experiment Procedure

Heart failure due to acute myocardial infarction, as a significant public health issue, is one of the leading causes of mortality and morbidity worldwide [46]. Non-invasive imaging in small animals, like rat and mouse myocardial infarction models, plays an essential role in pre-clinical research in this area and is used to explore cardiac pathophysiology and infarction assessment. There are multiple imaging modalities used detection and assessment of myocardial infarction severity and size, like echocardiography, SPECT, ultrasound, MRI. Magnetic resonance imaging (MRI) can provide accurate anatomical and functional measurements for infarction but is limited in the physiologic view of the vasculature disease [47]. Quantification of myocardial infarction by using Single-photon emission tomography (SPECT) with 99mTc-sestamibi or high-resolution SPECT is also available; however, there are some technical limitations such as low spatial resolution [48, 49].

When compared with SPECT, PET, as a thriving technology with high sensitivity, has a feasibility of quantitative measurements of the cardiovascular system [25]. Like Rubidium-82 [50], 13N-ammonia [51], and 15O water, but all of them have a clinical application due to the short half-life. 18F-labeled tracers became an attractive way to measure due to their ideal half-life [52]. FDG has a wide application in clinical in quantitative measurements of cardiovascular activity. The purpose of this chapter is to see whether RBC containing the radioactive tracer known as FDG can be used to indirectly look at blood perfusion and

microvascular dysfunction in infarcted myocardium in a surgical infarction rat heart model using an imaging technique known as positron emission tomographic (PET) imaging compare to pure FDG PET imaging and pathology TTC staining analysis. Specifically, the rats undergo surgery to tie off an artery supplying the rat heart muscle (the "left coronary artery") in order to induce cellular injury or death in the portion of the heart muscle that is supplied by the left coronary artery. The rats then undergo PET imaging with the FDG-labeled rat blood cells. It is hypothesized that PET imaging of FDG-labeled rat red blood cells in the rat heart would show a relative decrease in the vascularity to the infarcted portion of the rat heart downstream from the ligated coronary artery when compared to the adjacent uninjured heart muscle.

Rats also undergo PET imaging with regular free FDG and pathology Triphenyl tetrazolium chloride (TTC) staining analysis. The purpose of imaging these rats with regular FDG is that regular FDG can also be used to identify the location of heart attacks, as damaged rat heart muscle has relatively decreased metabolic activity compared to the healthy heart muscle, and heart muscle uptake of regular FDG is proportional to the degree of metabolic activity. The Rats undergo surgical ligation of the left coronary artery through an open intercostal approach, performed at an outside facility by the commercial vendor Envigo, which has extensive experience in coronary artery ligation of mice and rats.

After the all PET/SPECT imaging has been completed, the rat was sacrificed, and the heart was removed. The heart was then stained with 2,3,5-Triphenyl tetrazolium chloride (TTC) (Sigma Aldrich, St. Louis, MO), used by pathologists to identify infarcted myocardium. Successful imaging of injured heart muscle using FDG-labeled rat red blood cells would confirm the potential of this technique for characterizing heart attacks in patients with PET imaging. PET imaging of myocardial infarctions using this technique would represent a significant advance

over current SPECT-based myocardial perfusion imaging methods done routinely in the clinical setting, as current clinical 3D-PET scanners have both greater tracer sensitivity (50X) and better anatomic spatial resolution than typical clinical SPECT cameras.

Rats are imaged 1-6 weeks after surgery, depending on the results of the initial experiments. Rats are intravenously injected with the FDG-labeled erythrocytes through a tail vein catheter. Rats undergo microPET/CT imaging after injection of free FDG via tail vein catheter. Free FDG PET imaging should identify the location of the myocardial infarction as areas of decreased tracer activity, as infarcted myocardium will have decreased or absent FDG metabolic uptake. The location of these sites of decreased/absent FDG uptake was compared to the identified sites of decreased myocardial vascularity seen on the FDG-labeled erythrocyte PET images.

4.2 Materials and Method

All experiment procedures were approved by the University of South Florida (USF) Institutional Animal Care and Use Committee (IACUC). All experiments were performed in accordance to federal regulations and USF IACUC principles and procedures. All the chemicals obtained from Sigma Aldrich, St. Louis, MO, unless specified. A total of twelve of 4-8 weeks-old male Sprague Dawley (SD) rats were used, including four health male rats and six myocardial infarction rats created by using a standardized surgical ligation technique of the proximal rat left anterior descending artery with ~ 40% ejection fraction (EF) (Envigo, Indianapolis, IN).

4.3 ^{18}F-FDG Labeled RBC

The labeling procedure is pretty close to our previous study; much more details, please find in our previous research[53]. About 500-1000 μl blood was collected in heparin phlebotomy tube through the rat saphenous vein and stored in a 37 ˚C tissue culture incubator (Sanyo

Scientific) for 1-2 hours to increase the glucose depletion. After that, rat erythrocytes were centrifuged 1000 g for 10 minutes, and the remaining plasma and buffer coat residual were gently removed. The remaining red blood cell pellets were gently resuspended in 4X volume of filter-sterilized "1X EDTA" solution and centrifuged 1000g for 10 minutes. And the wash buffer was gently aspirated, and 100 µl 5X EDTA solution and 50 µl deionized water were then added to the 250 µl washed erythrocytes. Finally, 100 µl (37–74 MBq) USP grade ^{18}F-FDG (Cardinal Health, Tampa, FL) to a final volume of 500 µl. Samples were incubated in 37 ˚C for 30 minutes, centrifuged three times, and washed three times with 12 x volume of 1x EDTA/5mM glucose solution. ^{18} F-FDG labeled RBC PET/CT imaging was performed first, and then the free 18F-FDG PET//CT image was obtained the following week. After image processing, the rat was sacrificed, and the heart was excised intact, and saline flushed for pathology staining by 2,3,5-Triphenyl tetrazolium chloride (TTC) (Sigma Aldrich, St. Louis, MO) [54]. The rat was sacrificed, took out the heart, flushed with saline to wash away the remaining blood in the rat ventricular chamber, and then incubated in -20 ˚C freezer for 30 minutes for easy slicing. The frozen rat heart was cut into 2 mm transverse-slices in a 3-D printed rat heart mold for uniform transverse sectioning, incubated in 1% TTC (Sigma Aldrich, St. Louis, MO) buffer solution in 37 ˚C bath incubator for 20-30 minutes. The stained myocardial slices were then treated with 10% formalin for 20-30 minutes [55]. The formalin-treated heart slices were pictured.

4.4 Small Animal PET/CT Imaging

Similar imaging procedure as we previously study, much more details can be found in the paper by Wang *et al* [40]. 500-1000 µl of rat blood was drawn through saphenous venous plexus puncture and collected into the heparinized blood collection tube. The rat was anesthetized via a nosecone manifold under 2-4% inhalational isoflurane. Insert a tail vein

micro-catheter into one of the dilated rat tail veins after warm the rat tail. The rat was secured onto the micro-PET/CT scanner bed under 2-4% inhalational isoflurane anesthesia via a nose-cone manifold. 250-500 µl of FDG-labeled RBC suspension (the amount of activity range from $3.7x10^7$-$1.01x10^8$ Becquerel) was injected slowly into the rat through the tail vein microcatheter. Acquire ECG-gated the whole body images of the rat, followed by CT calibration images. PET/CT image acquisition parameters will depend upon the particular experimental indications and unique imaging platform set up at a given institution; thus, the following is a description of the protocol used at our institution. Place electrocardiogram (ECG) leads on two front limbs and one hind limb of the mouse (ground lead on a rear leg) for ECG gated PET imaging. The signals detected by these electrodes are recorded during the 20 minute period time by BioVet® (m2m Imaging) physiological monitoring and heating system.

4.5 PET Image Analysis

The protocol used at our institution is as the following description. Analyze the whole body PET images of the rat using Inveon Workstation Software (Siemens Medical Inc., Knoxville, Tennessee). For 3D PET and 4D PET data sets, manually select multiple volumes of interest (VOI) based on corresponding CT images for the following organs heart and the brain. Voxel activities are represented in standardized uptake values (SUV). Plot dynamic activity curves for VOIs using dynamic 3D PET data set for each animal. The 4D PET data are used for defining cardiac function. First, segment the heart on CT images based on anatomical features, then transfer the segmented volume (cardiac PET VOI) for image co-registration. Images are represented as maximum intensity projection (MIP) reconstructions of the source data. ECG guided binning of PET MIP images can be performed to obtain pseudo-dynamic images of mouse cardiac contractility.

4.6 Myocardial Infarction Size Measurement

The rat heart slices are stained by TTC, the viable tissue stained with red and infarcted myocardium stained as white. The pictures were analyzed by the “color threshold” mode to measure infarcted differentiate from viable tissue with ImageJ software (National Institutes of Health). Left ventricular short axis images were obtained from both FDG images and FDG RBCs images. Co-register RBC to Free-FDG. Select the same slice from both Free-FDG and RBC (select a slice where the defect is most visible). After axial segmentation of the left myocardium, the same slices were chosen from both FDG and RBC PET images for the same rat. Setting threshold the low signal in the heart (red). The low signal is the heart defected muscle. Percentage = (area of the defected muscle(red))/(area of all muscle). The infarct size was shown in percentage.

Segment heart muscle manually and extract activity (i.e., intensities) in the segmented heart region. And then, divide the extracted intestines into three segments, High, medium, and low. This is achieved by finding two thresholds using Otsu thresholding algorithm[56]. The low segment (i.e., region with low activity) is considered as the muscle defect. The percentage was showed by infarcted percentage= (area of the defected muscle(low))/ (area of all muscle). The other two regions, high and medium, are considered as normal heart muscles.

4.7 Results

Pathology analysis: the rats have successfully induced infarction after ligating the left descending artery. As showed in Figure 4.1, the black arrow indicated the ligation site, and the blue arrow pointed to the infarct area located at the left ventricular wall. As seen in Figure 4.4, the transverse sliced rat heart TTC staining results from rats 1-6. As results showed, there was significant scar area and atrophy at the left ventricular wall. The infarcted percentage measured

by TTC staining ranges from 21.35% to 31.90%. RBC FDG and free FDG PET imaging: after the axial segmentation of the left myocardium, the same transverse slices were chosen from both FDG and RBC PET images for the same rat.

The FDG labeled RBC PET images indicated that the decreased area myocardial vascularity correlated with both the area of decreased metabolic activity in free FDG PET images and the area of myocardial on tissue staining, as seen in Figure 4.2, A: short axial views of the left myocardial wall from FDG PET image, the triangle symbols indicate the decreased metabolic activities in the left ventricular wall. B: short axial views of the left myocardial wall from RBC PET image; the triangle symbols indicate the decreased vascularity in left ventricular muscles. The areas were highly correlated between the images of decreased metabolism and decreased vascularity.

Infarction percentage measurement: the RBC PET images provided a feasible way to estimate myocardial infarction (MI) size in vivo. After the axial segmentation of the left myocardium, the same transverse slices were chosen from both FDG and RBC PET images for the same rat. The same procedure applied to TTC pathology staining, the same transverse slice was chosen from the same rat; after the TTC staining, the MI size was measured, as in Figures 4.3 & 4.4. Table. 4.1 showed results of MI size measurement based on RBC, FDG PET images, and TTC pathology staining, separately.

As seen in Figure 4.5, Bland-Altman analysis was performed of MI size assessed by FDG and TTC, the difference between RBC and FDG measurements, and mean values. The mean difference between FDG and TTC measurement was 0.91, and the individual measurement differences are almost distributed in a narrow range around the mean. As seen in Figure 4.6, Bland-Altman graphic for comparison of MI size assessed by RBC and TTC. The mean

difference between TTC hispatology and RBC measurement was 7.875, and the individual measurement differences are almost distributed in a narrow range around the mean.

We then visually thresholded the activities into “low”, “medium” and “high” ranges. Some rats showed a “medium” range of activity in the peri-infarct areas of the FDG RBC PET images with otherwise viable metabolism on FDG images, suggestive of reduced per-infarct perfusion in “hibernating” (poorly contractile, but otherwise viable) myocardium in these regions. The decreased perfusion activity in the peri-infarct was correlated with the lower coronary flow reserve values finding in non-infarct-related arteries as previously reported [57]. Meanwhile, functional disorders in non-culprit coronary arteries were usually present in acute myocardial infarction patients [58].

The abnormalities physiology of the peri-infarct myocardial region, like the cardiovascular event and widespread inflammation, were discussed in the previous study [59]. The "intermediate" threshold signal in the infarction rat hearts should correspond to the peri-infarct distribution of the coronary arteries in the heart. Also, we observed that these peri-infarct areas with intermediate FDG RBC signal show relatively "normal" metabolic FDG uptake, suggesting that this could be "hibernating" myocardium.

4.8 Figures and Tables

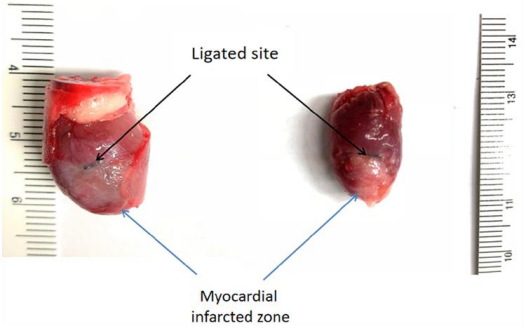

Figure 4.1 A simple example for rat heart after ligation of left descending arteries.

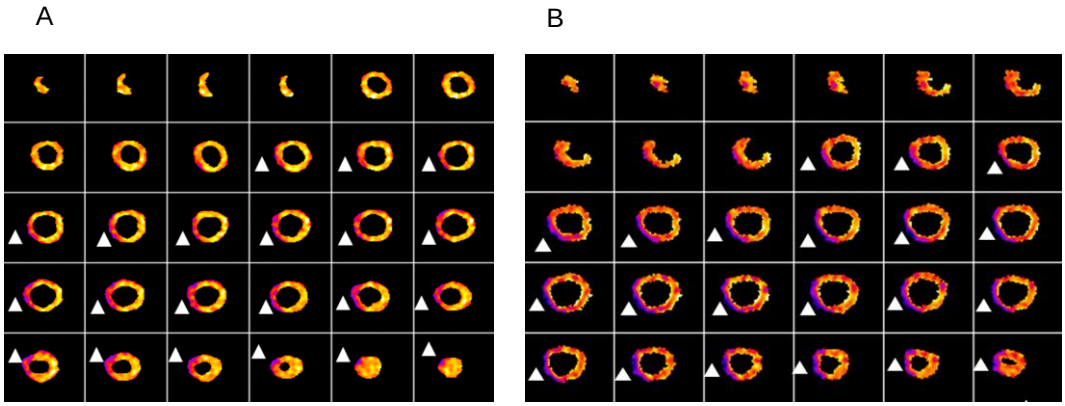

Figure 4.2 The images demonstrate the shorts axial views of the left myocardium for both FDG and RBC PET images. A: short axial views of the left myocardial wall from FDG PET image, the triangle symbols indicate the decreased metabolism activities in the left ventricular wall. B: short axial views of the left myocardial wall from RBC PET image; also, the triangle symbols indicate the decreased blood perfusion in left ventricular muscles. They were highly correlated for the same area decreased metabolism and blood perfusion activities.

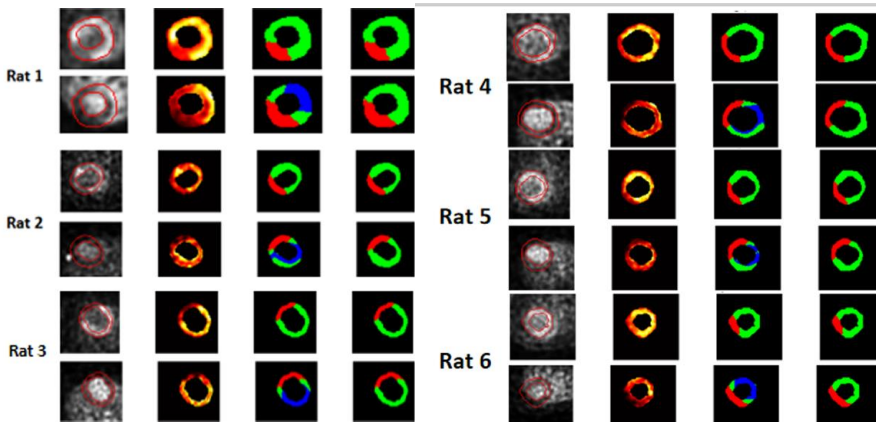

Figure 4.3 Same short axial views of Myocardial Infarction rats (number 1-6) cardiac PET images by FDG and RBC PET imaging, separately. After axial segmentation of the left myocardial, the same slices were chosen from both FDG and RBC PET images for the same rat. Automatically threshold the low signal in the heart (red). The low signal is the heart defected muscle. Percentage = (area of the defected muscle(red))/ (area of all muscle). The infarct size was shown in percentage. The MI size results were highly correlated between FDG and RBC PET images.

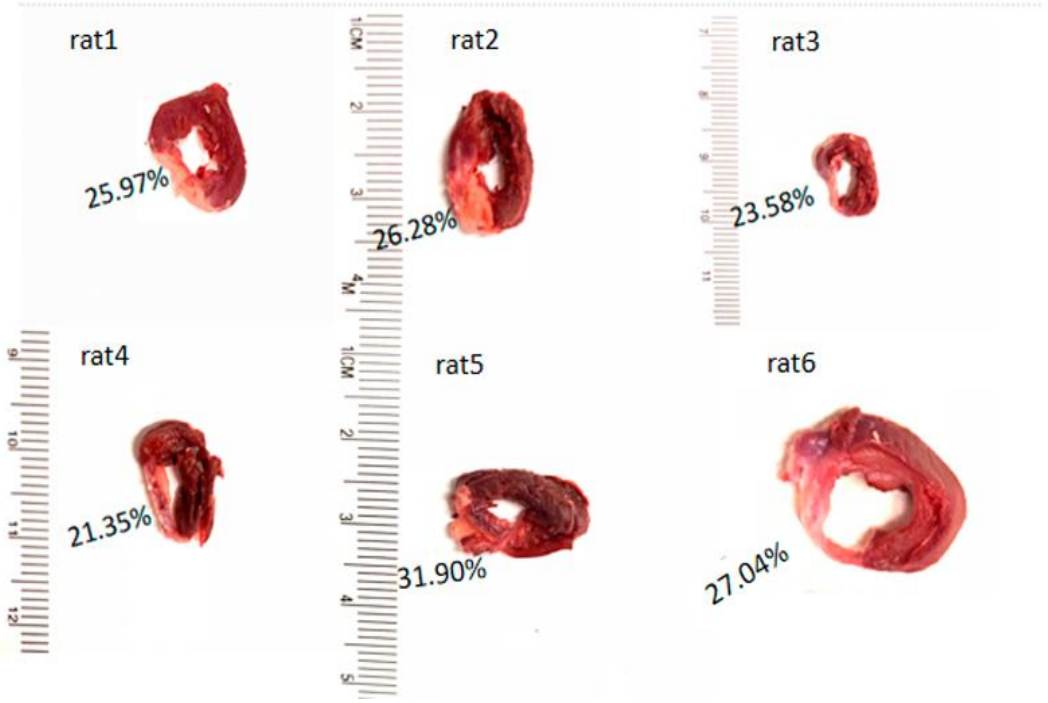

Figure 4.4 Transverse sliced rat heart TTC staining results from rat 1-6. As results showed, there was a significant scar area and variable atrophy at the left ventricular wall.

Table 4.1 Results of MI size measurement based on RBC, FDG PET images, and TTC pathology staining, separately.

	FDG%	RBC%	TTC%
1	24.38%	37.19%	25.97%
2	29.19%	29.49	26.28%
3	25.46%	32.85%	23.58%
4	29.26%	29.81%	21.35%
5	27.46%	35.39%	31.90%
6	25.62%	38.64%	27.04%
Mean ± S.E.	26.93%±0.83%	33.89%±1.56%	26.02%±1.45%

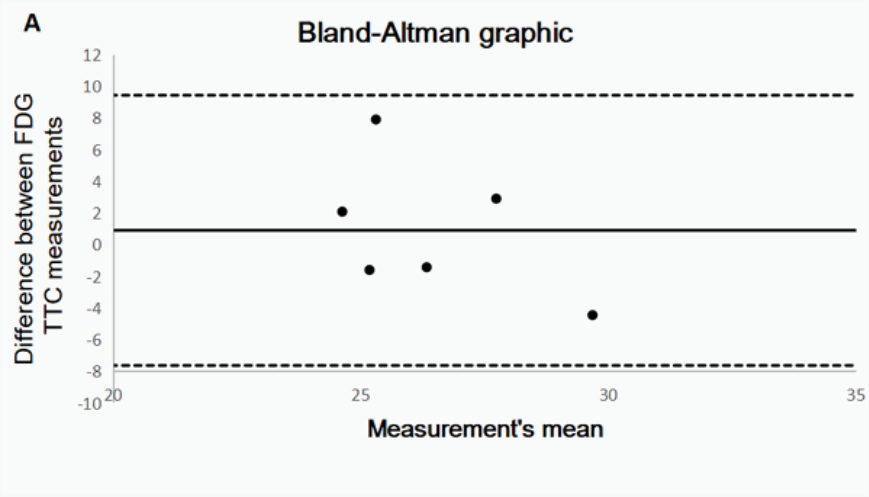

Figure 4.5 Bland-Altman graphic for comparison of MI size assessed by FDG and TTC, the difference between RBC and FDG measurements, and mean values.

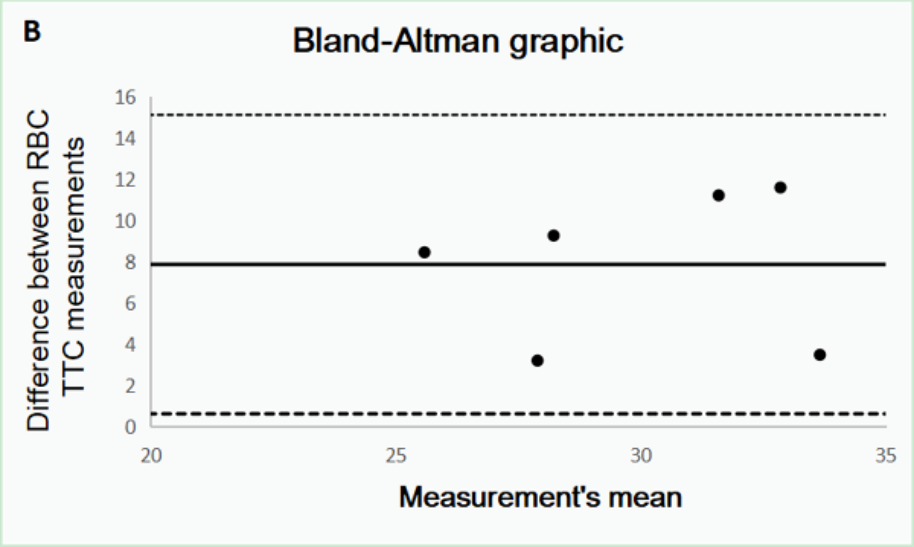

Figure 4.6 Bland-Altman graphic for comparison of MI size assessed by RBC and TTC, the difference between RBC and TTC measurement, and their mean values.

4.9 Discussion

Microvascular disease (MVD) refers to vascular diseases that primarily affect the small arteries, venule, and capillaries in various organs, especially in vital organs like the brain, heart, and kidney. It is a cause of cardiac ischemia, angina, dementia, stroke, and kidney dysfunction.

Currently, there is a relative dearth of imaging modalities that readily characterize microvascular dysfunction, outside of specific indications such as coronary artery catheter-based measurements such as Index of Microcirculatory Resistance (IMR). Other non-invasive cardiovascular imaging modalities are used to quantify blood flow and have an advanced understanding of microvascular dysfunction; nevertheless, most of these suffer from particular limitations, restricting use outside of specialized academic centers.

This work demonstrates the feasibility of 18F-FDG labeling RBC as a novel perfusion tracer for evaluation of the total myocardial microvascular volume under both rest and pharmacologic stress conditions and imaging the microvascular abnormalities associated with infarcted myocardium. Furthermore, this technique is able to approximate the location of infarction on the myocardial wall short axial views of 18F-FDG RBC PET imaging. The axial views of the area of decreased left ventricular myocardial vascularity on FDG RBC PET images closely matched the deceased myocardial metabolism activity on free FDG PET images as well as the infarcted myocardium on pathology tissue sampling. FDG RBC PET could be helpful for diabetic heart disease and other microvascular disease imaging. The data presented here suggests that FDG RBC PET imaging shows promise as a clinical imaging test for assessing cardiac perfusion and microvascular dysfunction.

Chapter 5: Myocardial Microvascular Dysfunction Measurement in Diabetic Rats

5.1 Research Purpose and Study Procedure

Diabetes mellitus (DM) is a long-term multifactorial disease associated with various vascular complications and became a nationwide health issue and is one of the leading causes of death in diabetic patients [60]. Diabetes is always associated with both microvascular and macrovascular complications and is a multifactorial disease associated with a number of microvascular (cardiomyopathy, retinopathy, neuropathy, and nephropathy) and macrovascular (ischemic heart disease, cerebrovascular disease, and peripheral vascular diseases) complications [61-64]. DM can develop many chronic complications, including heart attack and stroke, kidney failure, leg amputation, vision loss, and nerve damage [62, 65]. Moreover, diabetic mellitus can also lead to pulmonary vascular disease [66]. Cardiomyopathy of the diabetic is a major cause of heart failure nationwide [67]. The microvascular abnormalities in diabetic cardiomyopathy are still unclear. Diabetes-induced endothelial dysfunction is a critical and initiating factor in the genesis of diabetic vascular complications.

Streptozotocin (STZ) is an antibiotic that produces pancreatic islet β-cell destruction, leading the animal to experience insulin deficiency [68]. Furthermore, it is widely used in experiments to induce type 1 diabetes mellitus. In this work, we characterize myocardial vascularity in a streptozotocin-induced diabetic rat model. Rats were randomly divided into two groups. One group of 5 rats received 1-2 intravenous tail vein injections 40 mg/kg STZ [69, 70]. The onset and severity of diabetes were confirmed by weekly measurements of peripheral blood

glucose by needle prick. Moreover, weekly blood drawn for blood glucose concentration measurement were conducted on fasted rats. The other four rats will serve as normal age-matched controls. For each rat, 0.5 -1.0 cc's of blood were drawn either via saphenous or subclavian vein. The red blood cells from this blood sample were labeled with FDG and re-injected back into the same rat immediately prior to all PET imaging studies.

The mean purpose of this study is to see whether FDG labeled RBC PET imaging technique could be used to image vascularity in the heart muscle, brain, and other vessels in diabetic rats. The rats undergo PET imaging with the FDG-labeled rat blood cells. It was anticipated that PET imaging of FDG-labeled rat red blood cells would show a relative decrease in the total vascularity of the heart and when compared to the normal age-matched rats without diabetes.

The PET imaging experiments were conducted in rats from both groups at three month intervals to 1 year of age in the exact same manner, for the conditions described below: MicroPET/CT imaging before and after giving the cerebrovascular dilating drug Acetazolamide. MicroPET/CT imaging before and after giving the myocardial vascular dilating drug Regadenoson.

The severity of diabetic cardiomyopathy and other diabetic complications depends on the severity of the streptozotocin-induced pancreatic injury. The progression of diabetic cardiomyopathy is known to follow steps, with the development of left ventricular (LV) diastolic dysfunction and ventricular hypertrophy by eight weeks, followed by the development of LV systolic dysfunction, then decompensated heart failure. FDG RBC PET imaging of the heart of the first diabetic rats was performed 4-8 weeks after drug treatment to determine which time interval is optimal for detection of damage to the myocardial microvasculature. Once rats have

been found to have decreased myocardial microvascular density and impaired myocardial response to vasodilator challenge with regadenoson, rats were euthanatized. We anticipated that these findings would be detectable prior to the development of heart failure in most of these rats. Rats found to have developed decompensated heart failure were euthanatized.

Continuous inhalational anesthesia with isoflurane via nose cone manifold is required to minimize movements of the rat to allow for good signal acquisition by the PETCT imaging system during imaging experiments. For imaging data acquisition, rats were induced with isoflurane in a plastic anesthesia chamber with scavenging. They were then immediately placed into a rat-suitable holder in the PETCT scanner, outfitted with a nose cone inhalant anesthesia and scavenging system. The depth of anesthesia is normally assessed by using reflexes associated with an interdigital pinch.

After a rat had been intravenously injected with either pure FDG or FDG labeled-rat erythrocytes, the rat was placed under inhalational anesthesia into the Siemens microCT/PET/SPECT scanner in the Moffitt SAIL. The tail vein catheter is placed by appropriate Moffitt vivarium staff using a standardized procedure. After catheter placement, approximately 200 microliters of a sterile heparin flush solution (10 I.U. USP grade heparin/ml sterile PBS) are injected into the catheter hub to minimize clotting. Subsequent cell and drug injection through the catheter were followed by an injection of 200 microliters of heparin flush solution. The injection of cells was performed slowly over a period of 1-3 minutes. Following administration of the labeled red blood cells, rats underwent microPET/CT imaging for 15-30 minutes. 25 microgram/kg dose of Regadenoson (100 microliter volume) was then injected through the tail vein catheter, and the rat underwent additional microPET/CT imaging for 15-30 minutes.

5.2 Results

The diabetic group rats have pretty similar body weight and glucose level to the normal controls at baseline, body weight (342.2±32.4 vs. 345.2±34.3, p=0.1516), glucose level (120.4±5.9 vs. 119.4±7.7, p=0.4162), see Table 5.1. After STZ injection, the diabetic rats' blood glucose level typically increased dramatically over 400 mg/dl within 2-3 days, and the bodyweight slightly dropped down. As shown in Table 5.1, one week after STZ injection, the diabetic rats' weight dropped down about 6% (320.8±33.8 vs. 342.2±32.4), and blood glucose level increased dramatically (473.8±48.2 vs. 120.4±5.9) compared with body weight and glucose level on the baseline. However, the control group rats' weight increased about 7% (370.6±32.5 vs. 345.2±34.3), but the blood glucose remained at the same level (125.2±5.9 vs. 119.4±7.7). The diabetic rats presented hyperglycemia, decreased body weight, and drank more water due to copious urine when compared with normal age control group rats.

The FDG RBC PET imaging was able to image diabetic rats' myocardial vascularity directly. As seen in Figure 5.1, the shorts axial views of the left myocardium for the diabetic rat and the shorts axial views of the left myocardium for the normal age control rat seen in Figure 5.2. The standardized uptake values (SUV) histograms of the diabetic rat heart and control rat heart in rest, stress, and difference as showed in Figures 5.3 & 5.4.

The increased percentage of activities was shown: (stress-rest)/rest in diabetic rats and control group rats, as shown in Tables 5.2 & 5.3, increased percentage between stress and rest condition myocardium. Compared with control group rats, the stress-induced increase in myocardial vascularity in diabetic rats is about 50% of the control group (18.82%±2.03% vs. 35.12%±1.91%, p=0.00039), seen in Table 5.4. The impairment in vasodilatory response in the diabetic group was statistically significant (two-tailed Wilcoxon Rank-Sum test: $U = 0 \leq 2$, $p <$

0.05, diabetic rat n = 5; normal control n = 5). However, the diabetic rats' blood glucose levels are much higher than the control group, but the mean body weight is about 100 gm less than the control group.

5.3 Figures and Tables

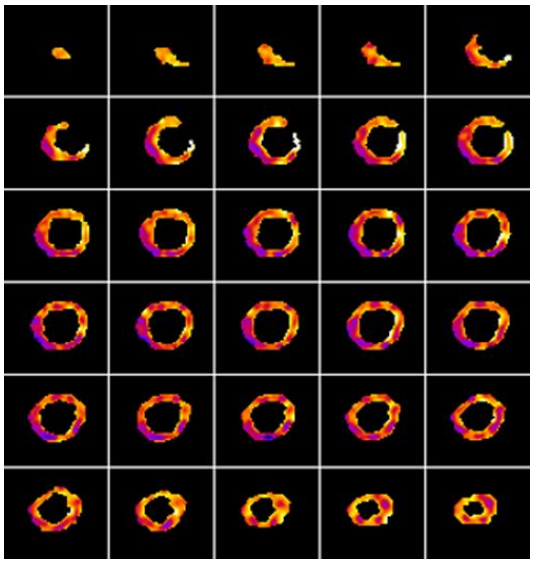

Figure 5.1 The images demonstrate the shorts axial views of the left myocardium for the diabetic rat.

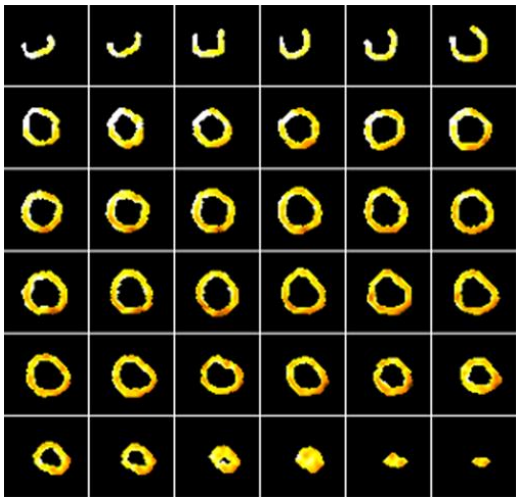

Figure 5.2 The images demonstrate the shorts axial views of the left myocardium for the normal age control rat.

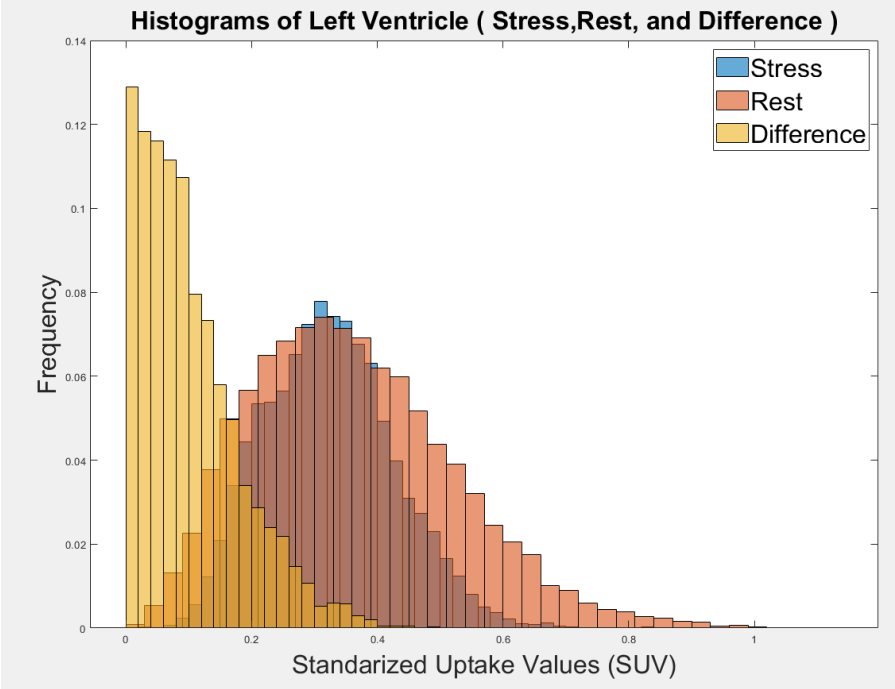

Figure 5.3 Standardized uptake values (SUV) histograms of the diabetic rat heart.

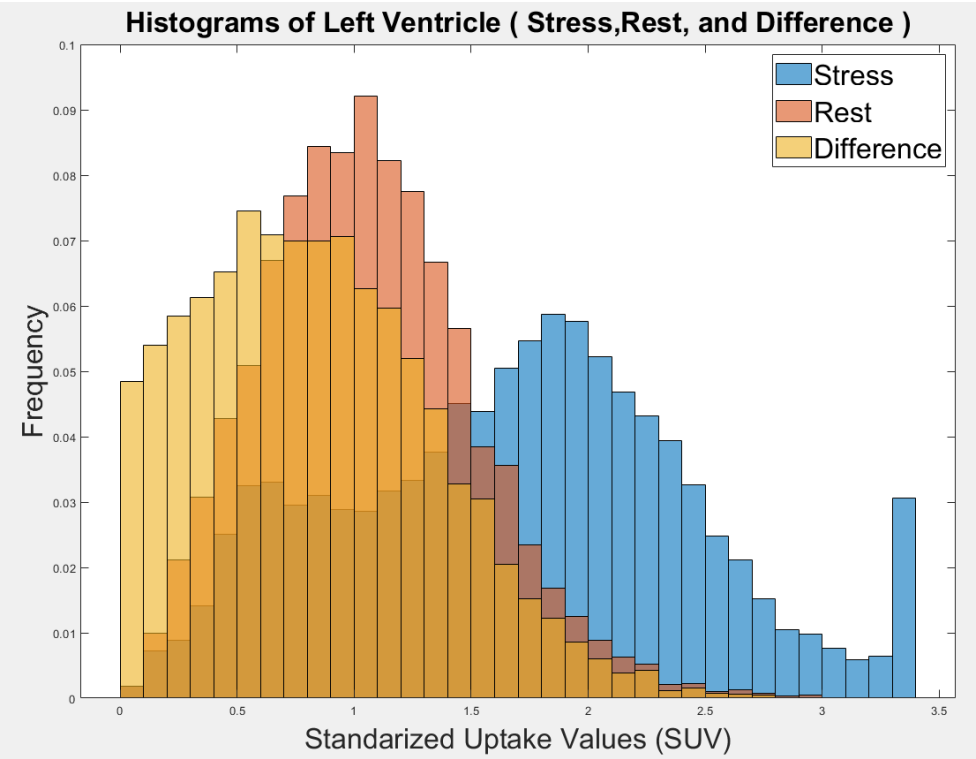

Figure 5.4 Standardized uptake values (SUV) histograms of the normal rat heart.

Table 5.1 Body weight and blood glucose of diabetic and control group

	Baseline			1 week		
	Control(n=5)	Diabetes(n=5)	P-value	Control(n=5)	Diabetes(n=5)	P-value
Body weight (g)	345.2 ± 34.3	342.2 ± 32.4	0.1516	370.6 ± 32.5	320.8 ± 33.8	0.0018
Blood glucose(mg/dl)	119.4 ± 7.7	120.4 ± 5.9	0.4162	125.2 ± 5.9	473.8 ± 48.2	<0.0001

Table 5.2 Measurement of the tracer activity intensity (BQ/ML) and SUV in both rest and stress conditions of the diabetic rat heart FDG PET imaging

Diabetic	Bq/ml (mean)	S.D.	SUV (mean)	S.D.
Rest	15871.33	5778.18	0.67	0.24
Stress	20854.55	8383.05	0.82	0.33
Difference	5779.65	5742.36	0.19	0.21

Table 5.3 Measurement of the tracer activity intensity (BQ/ML) and SUV in both rest and stress conditions of the control rat heart FDG PET imaging

Diabetic	Bq/ml (mean)	S.D.	SUV (mean)	S.D.
Rest	37468.94	14167.81	1.27	0.48
Stress	42433.04	15202.10	1.73	0.62
Difference	6084.36	6107.70	0.47	0.30

Table 5.4 Increased percentage between stress and rest condition myocardium. Body weight and blood glucose when imaging of diabetic and control group

	Increased percentage	Weight (g)	Blood glucose (mg/dl)
Control	35.12% ± 1.91%	428.3 ± 21.4	80.8 ± 28.4
Diabetes	18.82% ± 2.03%	310.5 ± 36.4	394.0 ± 86.6
P-value	0.00039	<0.0001	<0.0001

5.4 Discussion

In this work, the rats developed diabetes associated microvascular disease in the myocardium 5-8 weeks after STZ injection. The aims of this study were to try to image the brain, heart, and limb vascular damage after STZ induced type 1 diabetes. However, we did not detect vascular damage from the brain and limbs in the time period examined.

The complications associated with diabetic vascular dysfunction of diabetic are widely found in various organs like the heart, brain, kidney *etc*. Unlike atherosclerosis that leads to injury to the large epicardial vessels of the heart, diabetes affects all vessels throughout the body and is known for causing significant injury to the microvasculature. The FDG labeled RBC PET imaging provides a feasible way to examine changes from the myocardial microvascular disease over time as seen with the impaired vasodilatory response to the vasodilatory drug regadenoson. This technique would also be amenable to image-based absolute quantification of myocardial vascularity in the clinical setting. The FDG labeled RBC PET imaging provides an efficient way for cardiac vascular dysfunction. It has a great potential application for various organ dysfunction measurements. The complications associated with diabetic vascular dysfunction of diabetic are widely found in various organs like the heart, brain, kidney, etc.

Chapter 6: Discussion and Conclusion

FDG, as an FDA approved radiopharmaceutical, has a wide application in vivo glucose metabolism measurement. It is widely used in oncology PET imaging and regional glucose metabolism in the human brain. In this study, we provide an easy and direct procedure for labeling a small volume of RBC with FDG. It is a fairly rapid manual procedure that is relatively easy to perform and results in a labeling efficiency that is expected to be suitable for clinical PET imaging. FDG labeled RBC PET imaging is capable of visualizing the entire vasculature of various organs in rats. As the bulk of the total vascular volume of most organs is microvascular in size, FDG RBC PET imaging potentially offers a unique advantage over other common clinical imaging modalities, as it may be able to characterize the underlying microvasculature and associated disease of an organ of interest. To further demonstrate the abilities of this method, we show that changes in the rat myocardial vascular response to vasodilatory drugs can be visualized in normal and diabetic rats, and that response impairment is seen in the diabetic rats when compared to normal controls. As there are many microvascular pathologies that are not adequately assessed by current imaging modalities, it is of great interest to our group to advance the clinical translation of FDG-labeled RBC PET imaging. Evaluation of other microvascular disease types with this technique in small animal models shall also be pursued in the near future.

References

1. Benjamin Emelia, J., et al., *Heart Disease and Stroke Statistics—2019 Update: A Report From the American Heart Association.* Circulation, 2019. **139**(10): p. e56-e528.

2. Virani Salim, S., et al., *Heart Disease and Stroke Statistics—2020 Update: A Report From the American Heart Association.* Circulation, 2020. **141**(9): p. e139-e596.

3. *National Diabetes Statistics Report 2020: Estimates of Diabetes and Its Burden in the United States.* Medical Benefits, 2020. **37**(4): p. 3-4.

4. Taqueti, V.R. and M.F. Di Carli, *Coronary Microvascular Disease Pathogenic Mechanisms and Therapeutic Options: JACC State-of-the-Art Review.* Journal of the American College of Cardiology, 2018. **72**(21): p. 2625-2641.

5. Berry, C., et al., *Small-Vessel Disease in the Heart and Brain: Current Knowledge, Unmet Therapeutic Need, and Future Directions.* Journal of the American Heart Association, 2019. **8**(3): p. e011104.

6. Reis, S.E., et al., *Coronary microvascular dysfunction is highly prevalent in women with chest pain in the absence of coronary artery disease: Results from the NHLBI WISE study*. 2001, MOSBY-YEAR BOOK INC: United States. p. 735.

7. Wardlaw, J.M., et al., *Neuroimaging standards for research into small vessel disease and its contribution to ageing and neurodegeneration.* The Lancet Neurology, 2013. **12**(8): p. 822-838.

8. Nowroozpoor, A., D. Gutterman, and B. Safdar, *Is microvascular dysfunction a systemic disorder with common biomarkers found in the heart, brain, and kidneys? — A scoping review.* Microvascular Research, 2021. **134**.

9. Tonelli, M., et al., *Chronic Kidney Disease and Mortality Risk: A Systematic Review.* Journal of the American Society of Nephrology, 2006. **17**(7): p. 2034.

10. Rahman, H., et al., *Physiological Stratification of Patients With Angina Due to Coronary Microvascular Dysfunction.* Journal of the American College of Cardiology, 2020. **75**(20): p. 2538-2549.

11. Ford, T.J., et al., *Systemic microvascular dysfunction in microvascular and vasospastic angina.* European Heart Journal, 2018. **39**(46): p. 4086.

12. Sinha, A., H. Rahman, and D. Perera, *Ischaemia without obstructive coronary artery disease: the pathophysiology of microvascular dysfunction.* Current Opinion in Cardiology, 2020(6): p. 720.

13. Sucato, V., et al., *Ischemia in patients with no obstructive coronary artery disease: classification, diagnosis and treatment of coronary microvascular dysfunction.* Coronary Artery Disease, 2020(5): p. 472.

14. Fearon, W.F. and K. Yuhei, *Invasive Assessment of the Coronary Microvasculature: The Index of Microcirculatory Resistance.* Circulation: Cardiovascular Interventions, 2017. **10**(12): p. 1-11.

15. Berry, C., et al., *Fractional flow reserve-guided management in stable coronary disease and acute myocardial infarction: recent developments.* European Heart Journal, 2015. **36**(45): p. 3155.

16. Mathew, R.C., et al., *Cardiovascular Imaging Techniques to Assess Microvascular Dysfunction.* JACC: Cardiovascular Imaging, 2020. **13**(7): p. 1577-1590.

17. Firschke, C., et al., *Myocardial perfusion imaging in the setting of coronary artery stenosis and acute myocardial infarction using venous injection of a second-generation echocardiographic contrast agent.* Circulation, 1997. **96**(3): p. 959-967.

18. Porter, T.R., et al., *Improved myocardial contrast with second harmonic transient ultrasound response imaging in humans using intravenous perfluorocarbon-exposed sonicated dextrose albumin.* Journal of the American College of Cardiology, 1996. **27**(6): p. 1497-1501.

19. Appleton, C.P., et al., *Estimation of left ventricular filling pressures using two-dimensional and Doppler echocardiography in adult patients with cardiac disease: Additional value of analyzing left atrial size, left atrial ejection fraction and the difference in duration of pulmonary venous and mitral flow velocity at atrial contraction.* Journal of the American College of Cardiology, 1993. **22**(7): p. 1972-1982.

20. Nishimura, R.A., et al., *Noninvasive doppler echocardiographic evaluation of left ventricular filling pressures in patients with cardiomyopathies: A simultaneous doppler echocardiographic and cardiac catheterization study.* Journal of the American College of Cardiology, 1996. **28**(5): p. 1226-1233.

21. Schindler, T.H. and V. Dilsizian, *Coronary Microvascular Dysfunction: Clinical Considerations and Noninvasive Diagnosis.* JACC: Cardiovascular Imaging, 2020. **13**(1): p. 140-155.

22. Liu, A., et al., *RETRACTED: Diagnosis of Microvascular Angina Using Cardiac Magnetic Resonance.* Journal of the American College of Cardiology, 2018. **71**(9): p. 969-979.

23. Rossi, A., et al., *Dynamic Computed Tomography Myocardial Perfusion Imaging.* Circulation: Cardiovascular Imaging, 2017. **10**(4): p. e005505.

24. Morton, G., et al., *Quantification of Absolute Myocardial Perfusion in Patients With Coronary Artery Disease: Comparison Between Cardiovascular Magnetic Resonance and Positron Emission Tomography.* Journal of the American College of Cardiology, 2012. **60**(16): p. 1546-1555.

25. Kreissl, M.C., et al., *Noninvasive Measurement of Cardiovascular Function in Mice with High-Temporal-Resolution Small-Animal PET*. 2006, THE SOCIETY OF NUCLEAR MEDICINE INC: United States. p. 974.

26. Feher, A., et al., *Serial Assessment of Coronary Flow Reserve by Rubidium-82 Positron Emission Tomography Predicts Mortality in Heart Transplant Recipients.* JACC: Cardiovascular Imaging, 2020. **13**(1, Part 1): p. 109-120.

27. Munk, O.L., et al., *Determination of Regional Flow by Use of Intravascular PET Tracers: Microvascular Theory and Experimental Validation for Pig Livers.* Journal of Nuclear Medicine, 2003. **44**(11): p. 1862-1870.

28. Salerno, M. and A. Beller George, *Noninvasive Assessment of Myocardial Perfusion.* Circulation: Cardiovascular Imaging, 2009. **2**(5): p. 412-424.

29. Thrall, J.H., et al., *Clinical comparison of cardiac blood pool visualization with technetium-99m red blood cells labeled in vivo and with technetium-99m human serum albumin.* J Nucl Med, 1978. **19**(7): p. 796-803.

30. Hacker, M., et al., *Clinical validation of the gated blood pool SPECT QBS processing software in congestive heart failure patients: correlation with MUGA, first-pass RNV and 2D-echocardiography.* Int J Cardiovasc Imaging, 2006. **22**(3-4): p. 407-16.

31. Mohseni, S., et al., *Effects of filtration on right ventricular function by the gated blood pool SPECT.* Ann Nucl Med, 2015. **29**(4): p. 384-90.

32. Sadri, K., et al., *Nano Liposomes Labeled with (99m)Tc-HMPAO, a Novel Agent for Blood Pool Imaging.* Iran J Pharm Res, 2015. **14**(4): p. 981-8.

33. Liu, M., et al., *Novel Approach for (99m)Tc-Labeling of Red Blood Cells: Evaluation of (99m)Tc-4SAboroxime as a Blood Pool Imaging Agent.* Bioconjug Chem, 2017. **28**(12): p. 2998-3006.

34. Dong, H., et al., *The application of technetium-99m-red blood cell scintigraphy in the diagnosis of orbital cavernous hemangioma.* Nucl Med Commun, 2017. **38**(9): p. 744-747.

35. Rahmim, A. and H. Zaidi, *PET versus SPECT: strengths, limitations and challenges.* Nucl Med Commun, 2008. **29**(3): p. 193-207.

36. Nakazato, R., et al., *Myocardial perfusion imaging with PET.* Imaging Med, 2013. **5**(1): p. 35-46.

37. Lee, B.C., et al., *Optimization of temporal sampling for (82)rubidium PET myocardial blood flow quantification.* J Nucl Cardiol, 2017. **24**(5): p. 1517-1529.

38. Herrero, P., et al., *Assessment of myocardial blood flow using 15O-water and 1-11C-acetate in rats with small-animal PET.* J Nucl Med, 2006. **47**(3): p. 477-85.

39. Cysouw, M.C.F., et al., *Baseline and longitudinal variability of normal tissue uptake values of [(18)F]-fluorothymidine-PET images.* Nucl Med Biol, 2017. **51**: p. 18-24.

40. Wang, S. and J.W. Choi, *Imaging the Vasculature of Immunodeficient Mice Using Positron Emission Tomography/Computed Tomography (PET/CT) and 18F-fluorodeoxyglucose Labeled Human Erythrocytes.* Bio-protocol, 2019. **9**(19): p. e3391.

41. Dhalla, A.K., et al., *Tachycardia Caused by A_{2A} Adenosine Receptor Agonists Is Mediated by Direct Sympathoexcitation in Awake Rats.* Journal of Pharmacology and Experimental Therapeutics, 2006. **316**(2): p. 695-702.

42. Ray, A., et al., *Pharmacological studies on mechanisms of aminophylline-induced seizures in rats.* Indian J Exp Biol, 2005. **43**(10): p. 849-53.

43. Frankel, H.M., et al., *Effect of acetazolamide on cerebral blood flow and capillary patency.* J Appl Physiol (1985), 1992. **73**(5): p. 1756-61.

44. Bratosin, D., et al., *Novel Fluorescence Assay Using Calcein-AM for the Determination of Human Erythrocyte Viability and Aging*. 2005, WILEY - LISS: United States. p. 78.

45. Pretorius, E., J.N. du Plooy, and J. Bester, *A Comprehensive Review on Eryptosis.* Cellular Physiology and Biochemistry, 2016. **39**(5): p. 1977-2000.

46. Savarese, G. and L.H. Lund, *Global Public Health Burden of Heart Failure.* Cardiac failure review, 2017. **3**(1): p. 7-11.

47. Khafagy, R.T.M., et al., *Prognostic value of microvascular occlusion MRI quantification in assessment of reperfused myocardial infarction.* Egyptian Journal of Radiology & Nuclear Medicine, 2020. **51**(1): p. 1-10.

48. Liu, Z., et al., *Quantitative Analysis of Acute Myocardial Infarct in Rat Hearts with Ischemia-Reperfusion Using a High-Resolution Stationary SPECT System.* Journal of Nuclear Medicine, 2002. **43**(7): p. 933-939.

49. Oliveira, L.F.L.d., et al., *Quantificação da área de infarto usando-se SPECT de perfusão miocárdica de alta resolução em ratos / Myocardial infarction area quantification using high-resolution SPECT images in rats.* Arquivos Brasileiros de Cardiologia, 2013. **101**(1): p. 59-67.

50. Ghotbi, A.A., et al., *Rubidium-82 PET imaging is feasible in a rat myocardial infarction model.* Journal of Nuclear Cardiology, 2019. **26**(3): p. 798-809.

51. Inubushi, M., et al., *Nitrogen-13 ammonia cardiac positron emission tomography in mice: effects of clonidine-induced changes in cardiac work on myocardial perfusion.* European Journal of Nuclear Medicine and Molecular Imaging, 2004. **31**(1): p. 110-116.

52. Sherif, H.M., et al., *Evaluation of a novel (18)F-labeled positron-emission tomography perfusion tracer for the assessment of myocardial infarct size in rats.* Circ Cardiovasc Imaging, 2009. **2**(2): p. 77-84.

53. Choi, W.J., et al., *In vivo positron emission tomographic blood pool imaging in an immunodeficient mouse model using 18F-fluorodeoxyglucose labeled human erythrocytes.* PLoS ONE, 2019. **14**(1): p. e0211012-e0211012.

54. Bohl, S., et al., *Refined approach for quantification of in vivo ischemia-reperfusion injury in the mouse heart.* American Journal of Physiology: Heart & Circulatory Physiology, 2009. **297**(6): p. H2054-H2058.

55. Redfors, B., Y. Shao, and E. Omerovic, *Myocardial infarct size and area at risk assessment in mice.* Experimental and clinical cardiology, 2012. **17**(4): p. 268-72.

56. Otsu, N., *A Threshold Selection Method from Gray-Level Histograms.* IEEE Transactions on Systems, Man, and Cybernetics, Systems, Man and Cybernetics, IEEE Transactions on, IEEE Trans. Syst., Man, Cybern., 1979. **9**(1): p. 62-66.

57. Mejía-Rentería, H., et al., *Coronary Microcirculation Downstream Non-Infarct-Related Arteries in the Subacute Phase of Myocardial Infarction: Implications for Physiology-Guided Revascularization.* Journal of the American Heart Association, 2019. **8**(9): p. 1-11.

58. Díez-Delhoyo, F., E. Gutiérrez-Ibañes, and F. Fernández-Avilés, *Functional disorders in non-culprit coronary arteries and their implications in patients with acute myocardial infarction.* Trends in Cardiovascular Medicine, 2020. **30**(6): p. 346-352.

59. Hu, Q., et al., *Profound bioenergetic abnormalities in peri-infarct myocardial regions.* Am J Physiol Heart Circ Physiol, 2006. **291**(2): p. H648-57.

60. Cooper, M.E. and C.I. Johnston, *Optimizing Treatment of Hypertension in Patients With Diabetes.* JAMA, 2000. **283**(24): p. 3177-3179.

61. Knapp, M., X. Tu, and R. Wu, *Vascular endothelial dysfunction, a major mediator in diabetic cardiomyopathy.* Acta Pharmacol Sin, 2019. **40**(1): p. 1-8.

62. Clark, C.M. and D.A. Lee, *Prevention and Treatment of the Complications of Diabetes Mellitus.* New England Journal of Medicine, 1995. **332**(18): p. 1210-1217.

63. Paneni, F., et al., *Diabetes and vascular disease: pathophysiology, clinical consequences, and medical therapy: part I.* European Heart Journal, 2013. **34**(31): p. 2436-2443.

64. Cooper, M.E., et al., *Mechanisms of diabetic vasculopathy: an overview.* American Journal of Hypertension, 2001. **14**(5): p. 475-486.

65. Crawford, K., *Review of 2017 Diabetes Standards of Care.* Nursing Clinics of North America, 2017. **52**(4): p. 621-663.

66. Moral-Sanz, J., et al., *Different patterns of pulmonary vascular disease induced by type 1 diabetes and moderate hypoxia in rats.* Experimental Physiology, 2012. **97**(5): p. 676-686.

67. Tate, M., et al., *Insulin replacement limits progression of diabetic cardiomyopathy in the low-dose streptozotocin-induced diabetic rat.* Diabetes & Vascular Disease Research, 2017. **14**(5): p. 423-433.

68. Junod, A., et al., *Diabetogenic Action of Streptozotocin: Relationship of Dose to Metabolic Response.* The Journal of clinical investigation, 1969. **48**: p. 2129-39.

69. Furman, B.L., *Streptozotocin-Induced Diabetic Models in Mice and Rats.* Current Protocols in Pharmacology, 2015. **70**(1): p. 5.47.1-5.47.20.

70. Cosyns, B., et al., *Effect of streptozotocin-induced diabetes on myocardial blood flow reserve assessed by myocardial contrast echocardiography in rats.* Cardiovascular Diabetology, 2008. **7**: p. 1-10.

Appendix A: Copyright Permissions

The copyright permission below is for Chapter 2.

Copyright

Copyright for authors

Bio-protocol authors retain their copyright in the article.

License to publish

Bio-protocol is free to the research community (no publication fee; no access fee); advertising revenue from www.bio-protocol.org as well as its sister's website, www.bio-thing.com, Bio-protocol sister's website, will become the primary financial source to support Bio-protocol. Therefore, we ask our authors to sign an exclusive license that allows us to publish the article in Bio-protocol and any other Bio-protocol products (such as Bio-protocol's sister website, Bio-thing), and allows us to sublicense such rights and exploit all subsidiary rights. There is one exception to this: some content in Bio-protocol is published with an open-access (OA) license (see below).

Permissions

Permission for authors

If you are the author of the article that was published in Bio-protocol, you retain the rights to use the article and its contents as detailed in Bio-protocol's License to Publish.

Permission to use open-access (OA) content published in Bio-protocol

Bio-protocol articles deriving from eLife papers are distributed under the terms of the Creative Commons Attribution License (CC BY 4.0), which permits unrestricted use and redistribution provided that the original author and source are credited.

Articles that are published under a Creative Commons license will clearly indicate in the following locations which Creative Commons license governs its use:

1. In the html view of the article;
2. On the first page of the article PDF.

If your intended use of OA content is not covered by the applicable Creative Commons license, please submit a request to us following the instructions in the section of "Permission for non-authors" below.

Permission for non-authors

Everyone can freely access Bio-protocol content. However, if you want to reproduce/republish content from Bio-protocol and are not the author of that article, you must ask for our permission. We are usually happy to give permission to you free of charge if you are an individual, and your request is for personal and non-commercial purposes; or if you are a research institute or educational organization, and your request is for internal and non-commercial purposes. In any case, please e-mail us your request along with the following details:

1. Your name, institute, and title;
2. Your complete mailing address and phone number;
3. The content you wish to use including article title, authors' names, DOI, and specific data or portion of text.

Include the following information about your intended use:

1. Type of work in which our content will be used (e.g., book, journal, web portal etc.);
2. The rights you are seeking.

Please e-mail your request to permission@bio-protocol.org. All requests are reviewed and answered via email within 1 to 2 weeks after the submission of your request.

The copyright permission below is for chapter 3

Openness

The *PLOS ONE* community paved the way with open access. Now we're doing the same with open science.

PLOS applies the Creative Commons Attribution (CC BY) license to works we publish. Under this license, anyone may access, copy, distribute, or reuse these articles, as long as the author and original source are properly cited.

Throughout the peer review and publication process, the *PLOS ONE* research community enjoys additional opportunities to engage in openness and transparency, including enhanced author attribution and identification through the CRediT authorship taxonomy and ORCID iD, publicly posted protocols and data sets, optional preprint posting, and optional published peer review history.

About

Publication Fees

PLOS ONE publication fees vary based on article type and will be billed upon acceptance. Authors' ability to pay publication fees will never be a consideration in the decision whether to publish. You can find a full list of our publication fees and fee assistance information here.

Open Access

PLOS applies the Creative Commons Attribution (CC BY) license to works we publish. Under this license, authors agree to make articles legally available for reuse, without permission or fees, for virtually any purpose. Anyone may copy, distribute, or reuse these articles, as long as the author and original source are properly cited. Learn more.

Journal Impact and Article Metrics

PLOS does not consider Impact Factor to be a reliable or useful metric to assess the performance of individual articles. PLOS supports DORA – the San Francisco Declaration on Research Assessment – and does not promote our journal Impact Factors. We will provide the metric to individuals when specifically requested.

Appendix B: IACUC Approval

UNIVERSITY OF SOUTH FLORIDA
USF RESEARCH & INNOVATION

RESEARCH INTEGRITY & COMPLIANCE
INSTITUTIONAL ANIMAL CARE & USE COMMITTEE

MEMORANDUM

TO:	Jung Choi,
FROM:	Farah Moulvi, MSPH, IACUC Coordinator Institutional Animal Care & Use Committee Research Integrity & Compliance
DATE:	9/9/2019
PROJECT TITLE:	FDG-labeled erythrocyte PET imaging of rat myocardial, cerebral and peripheral perfusion in diabetic rat model
FUNDING SOURCE:	Non-Profit (Private Foundations, H. Lee Moffitt Cancer Center, etc.), For Profit (Industry Sponsored) or Other H Lee Moffitt Cancer Center
IACUC PROTOCOL #:	R IS00006926
PROTOCOL STATUS:	**APPROVED**

The Institutional Animal Care and Use Committee (IACUC) reviewed your application requesting the use of animals in research for the above-entitled study. The IACUC **APPROVED** your request to use the following animals in your **protocol for a one-year period beginning 9/9/2019:**

Rat: Wistar (2-4 months/250-350gm/male)	20

Please take note of the following:

• **IACUC approval is granted for a one-year period at the end of which, an annual renewal form must be submitted for years two (2) and three (3) of the protocol through the eIACUC system.** After three years all continuing studies must be completely re-described in a new electronic application and submitted to IACUC for review.

• **All modifications to the IACUC-Approved Protocol must be approved by the IACUC prior to initiating the modification.** Modifications can be submitted to the IACUC for review and approval as an Amendment or Procedural Change through the eIACUC system. These changes must be within the scope of the original research hypothesis, involve the original species and justified in writing. Any change in the IACUC-approved protocol that does not meet the latter definition is considered a major protocol change and requires the submission of a new application.

• **All costs invoiced to a grant account must be allocable to the purpose of the grant.** Costs allocable to one protocol may not be shifted to another in order to meet deficiencies caused by overruns, or for other reasons convenience. Rotation of charges among protocols by month without establishing that the rotation schedule credibly reflects the relative benefit to each protocol is unacceptable.

INSTITUTIONAL ANIMAL CARE AND USE COMMITTEE
PHS No. A4100-01, AAALAC No. 000434, USDA No. 58-R-0015

RESEARCH INTEGRITY AND COMPLIANCE
INSTITUTIONAL ANIMAL CARE & USE COMMITTEE

MEMORANDUM

TO:	Jung Choi,
FROM:	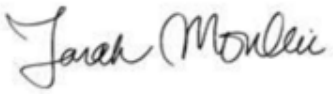 Farah Moulvi, MSPH, IACUC Coordinator Institutional Animal Care & Use Committee Research Integrity & Compliance
DATE:	5/18/2018
PROJECT TITLE:	FDG-labeled erythrocyte PET imaging of rat myocardial perfusion after acute myocardial infarction
FUNDING SOURCE:	H Lee Moffitt Cancer Center
IACUC PROTOCOL #:	R IS00005014
PROTOCOL STATUS:	**APPROVED**

The Institutional Animal Care and Use Committee (IACUC) reviewed your application requesting the use of animals in research for the above-entitled study. The IACUC **APPROVED** your request to use the following animals in your **protocol for a one-year period beginning 5/18/2018:**

Rat: F344 (CDF) rat (Charles River Lab) ((4-6 months/350 gm/male))	32

Please take note of the following:

• **IACUC approval is granted for a one-year period at the end of which, an annual renewal form must be submitted for years two (2) and three (3) of the protocol through the eIACUC system.** After three years all continuing studies must be completely re-described in a new electronic application and submitted to IACUC for review.

• **All modifications to the IACUC-Approved Protocol must be approved by the IACUC prior to initiating the modification.** Modifications can be submitted to the IACUC for review and approval as an Amendment or Procedural Change through the eIACUC system. These changes must be within the scope of the original research hypothesis, involve the original species and justified in writing. Any change in the IACUC-approved protocol that does not meet the latter definition is considered a major protocol change and requires the submission of a new application.

• **All costs invoiced to a grant account must be allocable to the purpose of the grant.** Costs allocable to one protocol may not be shifted to another in order to meet deficiencies caused by overruns, or for other reasons convenience. Rotation of charges among protocols by month without establishing that the rotation schedule credibly reflects the relative benefit to each protocol is unacceptable.

RESEARCH INTEGRITY AND COMPLIANCE
INSTITUTIONAL ANIMAL CARE & USE COMMITTEE

MEMORANDUM

TO:	Jung Choi,
FROM:	Farah Moulvi, MSPH, IACUC Coordinator Institutional Animal Care & Use Committee Research Integrity & Compliance
DATE:	11/7/2017
PROJECT TITLE:	PET imaging of rat myocardial perfusion using FDG-labeled rat erythrocytes
FUNDING SOURCE:	H Lee Moffitt Cancer Center
IACUC PROTOCOL #:	R IS00004376
PROTOCOL STATUS:	**APPROVED**

The Institutional Animal Care and Use Committee (IACUC) reviewed your application requesting the use of animals in research for the above-entitled study. The IACUC **APPROVED** your request to use the following animals in your **protocol for a one-year period beginning 11/7/2017:**

Rat: F344 (CDF) rat (Charles River Lab) (4-6 months/350 gm/male)	10

Please take note of the following:

• **IACUC approval is granted for a one-year period at the end of which, an annual renewal form must be submitted for years two (2) and three (3) of the protocol through the eIACUC system.** After three years all continuing studies must be completely re-described in a new electronic application and submitted to IACUC for review.

• **All modifications to the IACUC-Approved Protocol must be approved by the IACUC prior to initiating the modification.** Modifications can be submitted to the IACUC for review and approval as an Amendment or Procedural Change through the eIACUC system. These changes must be within the scope of the original research hypothesis, involve the original species and justified in writing. Any change in the IACUC-approved protocol that does not meet the latter definition is considered a major protocol change and requires the submission of a new application.

• **All costs invoiced to a grant account must be allocable to the purpose of the grant.** Costs allocable to one protocol may not be shifted to another in order to meet deficiencies caused by overruns, or for other reasons convenience. Rotation of charges among protocols by month without establishing that the rotation schedule credibly reflects the relative benefit to each protocol is unacceptable.

RESEARCH & INNOVATION • RESEARCH INTEGRITY AND COMPLIANCE
INSTITUTIONAL ANIMAL CARE AND USE COMMITTEE
PHS No. A4100-01, AAALAC No. 000434, USDA No. 58-R-0015
University of South Florida • 12901 Bruce B. Downs Blvd., MDC35 • Tampa, FL 33612-4799
(813) 974-7106 • FAX (813) 974-7091

Appendix C: List of Acronyms, Abbreviations, and Symbols

ACD	anticoagulant citrate dextrose
AIF	arterial input function
BQ/ML	becquerel per mililiter
Calcein-AM	acetoxymethl ester of calcein
CMR	cardic magnetic reasonace
CFR	coronary flow reserve
CT	computerize tomography
CTA	computed tomographic angiography
CVD	coronary microvascular dysfunction
DM	diabetes mellitus
ECG	electrocardiogram
FDG	18F-fluorodeoxyglucose
IMR	index of microcirculatory resistance
MBF	myocardial blood flow
mCi	millicuries
ml	mililiter
µl	micorliter
MIP	maximum intensity projection
MRA	magnetic resonance angiography
MVD	microvascular dysfunction

PET	positron emission tomography
PET/CT	positron emission tomography/computerized tomography
RBC	red blood cells
SPECT	single-photon emission computed tomographic
SUV	standardized uptake values
TTC	triphenyl tetrazolium chloride
VOI	volumes of interest